


Universal competitive spectral scaling from the critical non-Hermitian skin effect

Fang Qin (覃昉)¹,* Ye Ma (马烨)¹, Ruizhe Shen (申锐哲)¹, and Ching Hua Lee (李庆华)¹†
Department of Physics, National University of Singapore, Singapore 117551, Singapore

 (Received 3 January 2023; revised 23 March 2023; accepted 23 March 2023; published 26 April 2023)

Recently, it was discovered that certain non-Hermitian systems can exhibit qualitative different properties at different system sizes, such as being gapless at small sizes and having topological edge modes at large sizes L . This dramatic system-size sensitivity is known as the critical non-Hermitian skin effect (cNHSE), and occurs due to the competition between two or more non-Hermitian pumping channels. In this work, we rigorously develop the notion of a size-dependent generalized Brillouin zone (GBZ) in a general multicomponent cNHSE model ansatz, and found that the GBZ exhibits a universal $a + b^{1/(L+1)}$ scaling behavior. In particular, we provided analytical estimates of the scaling rate b in terms of model parameters, and demonstrated their good empirical fit with two paradigmatic models, the coupled Hatano-Nelson model with offset, and the topologically coupled chain model with offset. We also provided analytic result for the critical size L_c , below which cNHSE scaling is frozen. The cNHSE represents the result of juxtaposing different channels for bulk-boundary correspondence breaking, and can be readily demonstrated in non-Hermitian metamaterials and circuit arrays.

DOI: [10.1103/PhysRevB.107.155430](https://doi.org/10.1103/PhysRevB.107.155430)

I. INTRODUCTION

Non-Hermitian systems harbor a host of interesting physics not found in equilibrium systems, such as exceptional point sensitivity and robustness [1–17], enlarged symmetry classes [18–21], and intrinsically nonequilibrium topological phases [22–35]. Once thought to exist almost exclusively as mathematical constructs, these novel phenomena have one by one been experimentally demonstrated in the recent years, thanks to rapid technical advances in ultracold atomic gases [36–40], electrical circuits [41–53], photonic systems [11,23,54–62], coupled acoustic cavities [63–67], as well as other metamaterials [68–80].

A particularly intriguing type of non-Hermitian phenomenon is the breaking of conventional bulk-boundary correspondences (BBCs), which generically occurs whenever reciprocity is also broken. Topological BBCs relate boundary topological states with bulk topological invariants, and are cherished tenets in topological classification [81–86]. The most well-studied type of non-Hermitian BBC is the non-Hermitian skin effect (NHSE) [87–104], which is characterized by exponentially large boundary state accumulation that leads to very different energy spectra under open and periodic boundary conditions (OBCs and PBCs). To restore an effective bulk theory, the customary approach has been to define a generalized Brillouin zone (GBZ) with complexified momentum [91,105–112], such that quantities computed in the GBZ correctly correspond to physical observations.

Most interesting is the relatively little-understood scenario of *critical* NHSE (cNHSE) [113], where even the scaling properties of the system are drastically modified by non-

Hermiticity. For instance, the same metamaterial exhibiting cNHSE can behave qualitatively differently at different system sizes, such as being gapless (metallic) at small sizes but topologically insulating at large sizes [113–116]. Physically, such peculiar size-dependent transitions are due to the competition between multiple NHSE channels (nonreciprocity strengths) in the system; at different length scales, the same physical coupling can be “renormalized” to very different values dependent on the dominant NHSE channel. Due to their peculiar size dependency, the cNHSE systems also harbor different entanglement scaling laws [113] from those of other Hermitian and non-Hermitian phases [7–9,117–126].

In this work, we focus on addressing the following open question: How exactly can we understand cNHSE scaling behavior in terms of the GBZ, which is widely used for restoring the BBC in the thermodynamic limit? Specifically, we find that a cNHSE system of finite size can be accurately described through an “interpolated” GBZ that lies between the competing GBZs describing the same (but behaviorally distinct) system in the small and large size limits. Furthermore, this interpolation occurs at a rate obeying a universal exponential scaling law, with exponent inversely proportional to system size. Since the effective GBZ allows one to represent the system with a Hamiltonian with an effective Bloch description, this scaling law carries over into most physical properties of cNHSE lattices.

To motivate and substantiate our results, we consider a generic two-component ansatz for modeling a cNHSE system with two competing NHSE channels. Our ansatz encompasses the minimal model studied in Ref. [127], and showcases how some of its results can be generalized in the context of arbitrary NHSE channels. By subsequently specializing into two paradigmatic models, we provide detailed derivations of the universal $a + b^{1/(L+1)}$ scaling behavior governing the effective finite-size GBZ, where L is the system size, and

* qinfang@nus.edu.sg

† phylch@nus.edu.sg

a, b constants depending on the model details. We also provide detailed and empirically verified estimates of the lower critical system size L_c above which such a scaling relation holds.

We pause to briefly elaborate on the experimental prospects for the cNHSE models discussed in this work. Most directly, electrical circuits, i.e., “topoelectrical circuits” can be connected in very versatile manners, and are thus readily suited for their experimental implementation [41–53]. In general, operation amplifiers serve as almost perfectly linear components with asymmetric Laplacians [42], and are thus ideal building blocks for models with the asymmetric couplings necessary for cNHSE. Recently, the coupled Hatano-Nelson cNHSE model of this work has also been realized in an even simpler experimental circuit platform [52] involving only RLC circuit components since asymmetric couplings can be rendered symmetric via a basis rotation in this model. Circuit realizations can also be largely generalized to photonic platforms [55,128–134]. Coupled resonator arrays can be used to experimentally realize the arrays in our models, with the ring resonators [128] (which are the primary resonators) representing the sites in our model chains. Experimental values of the hoppings in such photonic systems are highly tunable, ranging approximately from 5 to 30 GHz [135,136]. The optical gain and loss in a photonic system can be used to experimentally realize the gain and loss in our non-Hermitian models.

The paper is organized as follows: In Sec. II, we set up the cNHSE formalism using a general two-component ansatz. Next, we illustrate our results through detailed calculations on two paradigmatic models, a coupled Hatano-Nelson model with energy offset (Sec. III) and a model with size-dependent topology (Sec. IV). We show how their OBC spectra and effective GBZs depend greatly on the system size, and provide quantitative derivations of their exponential scale dependence, as well as the critical system size above which such scaling holds. In Sec. V, we demonstrate the robustness of the scaling of imaginary energy against substantial disorder. Finally, we summarize the key findings in the discussion in Sec. VI.

II. GENERAL TWO-COMPONENT cNHSE ANSATZ

To understand the cNHSE phenomenon, we first review the concept of the GBZ. The GBZ formalism restores the BBC via a complex momentum deformation. For a momentum-space one-dimensional (1D) Hamiltonian $H(z)$ with $z = e^{ik}$, the GBZ corresponding to an eigenenergy E can be obtained from solving for $z = e^{ik}$ in the following characteristic Laurent polynomial [89,105]:

$$f(z, E) := \det[H(z) - E \mathbb{I}] = 0. \quad (1)$$

For E that does not coincide with any of the PBC eigenenergies, i.e., eigenvalues of $H(e^{ik})$ for real k , we must have complex $k = -i \ln z$. Such E lies in the OBC spectrum when the latter is very different from the PBC spectrum. It can be shown that [87,89,91,99,101,110] in the thermodynamic limit, the OBC eigenenergies are given by¹ solutions of k that are

¹This double degeneracy in $\text{Im}(k)$ is required for the state to vanish at two boundaries that are arbitrary far apart.

doubly degenerate in both $\text{Im}(k)$ and E : For such solutions, we define the GBZ as $\kappa(k)$, where the complex momentum deformation is given by $k \rightarrow k + i\kappa(k)$. In other words, we say that the conventional (Bloch) BZ is replaced by the (non-Bloch) GBZ defined by $z \rightarrow e^{ik} e^{-\kappa(k)}$.

To understand how the GBZ formalism needs to be modified in a cNHSE system, we start from a generic two-component ansatz cNHSE Hamiltonian, written in the component basis $C_{\mathbf{k}} = (c_{\mathbf{k},A}, c_{\mathbf{k},B})^T$ as

$$\mathcal{H}_g(z) = \begin{pmatrix} \mathcal{H}^{aa}(z) & \mathcal{H}^{ab}(z) \\ \mathcal{H}^{ba}(z) & \mathcal{H}^{bb}(z) \end{pmatrix} = \sum_{n=-n_-}^{n_+} \begin{pmatrix} h_n^{aa} & h_n^{ab} \\ h_n^{ba} & h_n^{bb} \end{pmatrix} z^n, \quad (2)$$

where $n_{\pm} \in \mathbb{Z}$, $z = e^{ik}$. In principle, cNHSE exists as long as \mathcal{H}^{aa} and \mathcal{H}^{bb} exhibit dissimilar inverse skin localization lengths $\kappa(k)$, and couplings $\mathcal{H}^{ab}, \mathcal{H}^{ba} \neq 0$. The former condition is equivalent to having asymmetric hoppings $h_n^{aa} \neq h_{-n}^{aa}$ and $h_n^{bb} \neq h_{-n}^{bb}$ for some n , as well as $h_n^{aa}/h_{-n}^{aa} \neq h_n^{bb}/h_{-n}^{bb}$.

To implement OBCs, we first Fourier transform to real space, where one obtains the real-space tight-binding Hamiltonian

$$H_{gr} = \sum_{i=1}^L \sum_{n=-n_-}^{n_+} C_i \begin{pmatrix} h_n^{aa} & h_n^{ab} \\ h_n^{ba} & h_n^{bb} \end{pmatrix} C_{i+n}, \quad (3)$$

where L is the system size, i.e., number of unit cells, $1 \leq n_{\pm} \leq L/2$, $C_i = (c_{i,A}, c_{i,B})^T$ with the annihilation (creation) operator $c_{i,\alpha}$ ($c_{i,\alpha}^\dagger$) on site α ($\alpha = A, B$) in cell i . For a real-space wave function $|\psi\rangle = (\psi_{1,A}, \psi_{1,B}, \psi_{2,A}, \psi_{2,B}, \dots, \psi_{L,A}, \psi_{L,B})^T$, we express the real-space Schrödinger equation $\mathcal{H}_{gr}|\psi\rangle = E_{\text{OBC}}|\psi\rangle$ as

$$\begin{cases} \sum_{n=-n_-}^{n_+} (h_n^{aa} \psi_{i+n,A} + h_n^{ab} \psi_{i+n,B}) = E_{\text{OBC}} \psi_{i,A}, \\ \sum_{n=-n_-}^{n_+} (h_n^{ba} \psi_{i+n,A} + h_n^{bb} \psi_{i+n,B}) = E_{\text{OBC}} \psi_{i,B}, \end{cases} \quad (4)$$

where \mathcal{H}_{gr} is the Hamiltonian matrix of H_{gr} in the basis $(C_1, C_2, \dots, C_L)^T$ and E_{OBC} is the eigenenergy under OBC. To relate to the complex momenta present in non-Hermitian skin modes, we solve the real-space Schrödinger equation via the ansatz

$$(\psi_{n,A}, \psi_{n,B})^T = \sum_j (\beta_j)^n (\phi_A^{(j)}, \phi_B^{(j)})^T, \quad (5)$$

where A, B are the site indices in the cell, and n represents the position of the cell (A,B) in the real space. Here, β_j are specific solutions to $z = e^{ik}$, and characterize the spatial localization of the boundary skin-localized wave function. By substituting Eq. (5) into (4), we can write the bulk eigenequation as

$$\begin{cases} \left[\sum_{n=-n_-}^{n_+} h_n^{aa} (\beta_j)^n - E_{\text{OBC}} \right] \phi_A^{(j)} + \sum_{n=-n_-}^{n_+} h_n^{ab} (\beta_j)^n \phi_B^{(j)} = 0, \\ \sum_{n=-n_-}^{n_+} h_n^{ba} (\beta_j)^n \phi_A^{(j)} + \left[\sum_{n=-n_-}^{n_+} h_n^{bb} (\beta_j)^n - E_{\text{OBC}} \right] \phi_B^{(j)} = 0. \end{cases} \quad (6)$$

Equation (6) can be recast into the energy dispersion characteristic equation

$$E_{\text{OBC}}^2 - \sum_{n=-n_-}^{n_+} (h_n^{aa} + h_n^{bb})(\beta_j)^n E_{\text{OBC}} + \left[\sum_{n=-n_-}^{n_+} h_n^{aa}(\beta_j)^n \right] \left[\sum_{n=-n_-}^{n_+} h_n^{bb}(\beta_j)^n \right] - \left[\sum_{n=-n_-}^{n_+} h_n^{ab}(\beta_j)^n \right] \left[\sum_{n=-n_-}^{n_+} h_n^{ba}(\beta_j)^n \right] = 0, \quad (7)$$

where we have labeled the solutions β_j with increasing magnitude $|\beta_1| \leq |\beta_2| \leq \dots \leq |\beta_{2M}|$. Here $M = n_- + n_+$.

$$\begin{vmatrix} F_1^{(a,1)} \beta_1 & F_2^{(a,1)} \beta_2 & \dots & F_{2M}^{(a,1)} \beta_{2M} \\ F_1^{(b,1)} \beta_1 & F_2^{(b,1)} \beta_2 & \dots & F_{2M}^{(b,1)} \beta_{2M} \\ \vdots & \vdots & \vdots & \vdots \\ F_1^{(a,n_+)} (\beta_1)^{n_+} & F_2^{(a,n_+)} (\beta_2)^{n_+} & \dots & F_{2M}^{(a,n_+)} (\beta_{2M})^{n_+} \\ F_1^{(b,n_+)} (\beta_1)^{n_+} & F_2^{(b,n_+)} (\beta_2)^{n_+} & \dots & F_{2M}^{(b,n_+)} (\beta_{2M})^{n_+} \\ G_1^{(a,1)} (\beta_1)^{L-(n_- - 1)} & G_2^{(a,1)} (\beta_2)^{L-(n_- - 1)} & \dots & G_{2M}^{(a,1)} (\beta_{2M})^{L-(n_- - 1)} \\ G_1^{(b,1)} (\beta_1)^{L-(n_- - 1)} & G_2^{(b,1)} (\beta_2)^{L-(n_- - 1)} & \dots & G_{2M}^{(b,1)} (\beta_{2M})^{L-(n_- - 1)} \\ \vdots & \vdots & \vdots & \vdots \\ G_1^{(a,n_-)} (\beta_1)^L & G_2^{(a,n_-)} (\beta_2)^L & \dots & G_{2M}^{(a,n_-)} (\beta_{2M})^L \\ G_1^{(b,n_-)} (\beta_1)^L & G_2^{(b,n_-)} (\beta_2)^L & \dots & G_{2M}^{(b,n_-)} (\beta_{2M})^L \end{vmatrix} = 0, \quad (8)$$

as derived in more detail in Appendix A. This determinant expression captures the constraints from OBCs at both boundaries. In general, it is a complicated expression, but can still be written explicitly in terms of β_j and E_{OBC} for the two-band ansatz:

$$F_j^{(a,i)} = \sum_{n=-(i-1)}^{n_+} (h_n^{aa} + f_j h_n^{ab})(\beta_j)^n - E_{\text{OBC}}, \quad (9)$$

$$F_j^{(b,i)} = \sum_{n=-(i-1)}^{n_+} (h_n^{ba} + f_j h_n^{bb})(\beta_j)^n - f_j E_{\text{OBC}}, \quad (10)$$

$$G_j^{(a,i)} = \sum_{n=-n_-}^{n_- - i} (h_n^{aa} + f_j h_n^{ab})(\beta_j)^n - E_{\text{OBC}}, \quad (11)$$

$$G_j^{(b,i)} = \sum_{n=-n_-}^{n_- - i} (h_n^{ba} + f_j h_n^{bb})(\beta_j)^n - f_j E_{\text{OBC}}, \quad (12)$$

where

$$f_j = \frac{\phi_B^{(j)}}{\phi_A^{(j)}} = \frac{E_{\text{OBC}} - \sum_{n=-n_-}^{n_+} h_n^{aa} (\beta_j)^n}{\sum_{n=-n_-}^{n_+} h_n^{ab} (\beta_j)^n} = \frac{\sum_{n=-n_-}^{n_+} h_n^{ba} (\beta_j)^n}{E_{\text{OBC}} - \sum_{n=-n_-}^{n_+} h_n^{bb} (\beta_j)^n}. \quad (13)$$

Importantly, the key property required for restoring BBCs, the complex momentum deformation (effective GBZ), does not require intimate knowledge of most of these β solutions. This is because fundamentally, the required complex deformation depends on the decay rate of the eigenstates, which turns out to depend only on two dominant β solutions. Below, we derive the precise conditions from the bulk eigenequations (6) as well as constraints from the OBCs $\psi_{-n,-,\alpha} = \dots = \psi_{-1,\alpha} = \psi_{0,\alpha} = \psi_{L+1,\alpha} = \psi_{L+2,\alpha} = \dots = \psi_{L+n_+,\alpha} = 0$ ($\alpha = A, B$; $1 \leq n_{\pm} \leq L/2$).

By eliminating $\phi_B^{(j)}$ in terms of $\phi_A^{(j)}$, we obtain $2M$ simultaneous linear equations in $\phi_A^{(j)}$ ($j = 1, 2, \dots, 2M$), which yield nonvanishing solutions only if the determinant

Equation (8) can be rearranged in a compact multivariate polynomial form

$$\sum_{P,Q} J(\beta_{i \in P}, \beta_{j \in Q}, E_{\text{OBC}}) \left[\prod_{i \in P} (\beta_i)^k \right] \left[\prod_{j \in Q} (\beta_j)^{k'} \right] = 0, \quad (14)$$

where $k = 1, \dots, n_+$, $k' = L - (n_- - 1), \dots, L$, sets P and Q are two disjoint subsets of the set $\{1, 2, \dots, 2M\}$ with M elements, respectively, and $J(\beta_{i \in P}, \beta_{j \in Q}, E_{\text{OBC}})$ is the E_{OBC} -dependent coefficient corresponding to a particular permutation of P and Q . By separating the product contributions of the β s which are exponentiated by L , we can extract out contributions that scale differently with L .

Furthermore, in the case $n_+ = n_-$ where the maximal left and right hopping distances are the same, Eq. (14) simplifies to

$$\sum_{P,Q} J(\beta_{i \in P}, \beta_{j \in Q}, E_{\text{OBC}}) \left[\prod_{i \in P} (\beta_i)^{L+1} \right] = 0. \quad (15)$$

In the thermodynamic limit, the large L in the exponents picks up the slowest decaying terms, and these would be the physically dominant contributions amidst the complicated jumble of terms. Specifically, in Eq. (15), we find that there are two leading terms proportional to $(\beta_M \beta_{M+2} \beta_{M+3} \dots \beta_{2M})^{L+1}$ and $(\beta_{M+1} \beta_{M+2} \beta_{M+3} \dots \beta_{2M})^{L+1}$, which yield in the limit of large

system size L

$$\left| \frac{\beta_M}{\beta_{M+1}} \right| \simeq \left| -\frac{J(\beta_{i \in P_1}, \beta_{j \in Q_1}, E_{\text{OBC}})}{J(\beta_{i \in P_2}, \beta_{j \in Q_2}, E_{\text{OBC}})} \right|_{E_{\text{OBC}}=E_\infty}^{\frac{1}{L+1}}, \quad (16)$$

where $P_1 = \{M+1, M+2, M+3, \dots, 2M\}$, $Q_1 = \{1, 2, 3, \dots, M\}$, $P_2 = \{M, M+2, M+3, \dots, 2M\}$, $Q_2 = \{1, 2, \dots, M-2, M-1, M+1\}$, $M = n_+ + n_-$, and L is the system size with $L \rightarrow \infty$. We emphasize that the form of this result (16) with $L \rightarrow \infty$ still holds for general higher-component or multiband models [see Eq. (B19)], albeit with more complicated J functions], as derived in Appendix B. The details are complicated, but physically, we expect qualitatively similar behavior because the critical NHSE essentially arises from the competition between the NHSE and the couplings, and with greater number of bands, we will have more avenues for the competition. But unless the model is fine tuned, we will generically still see the direct competition between pairs of bands, which thus reduces qualitatively to two-band behavior.

We comment on a few key takeaways from Eq. (16). Without any assumption on the detailed hoppings in the 1D tight-binding model, we showed how the requirement of satisfying OBCs at both ends generically led to Eq. (16), which relates $|\beta_M/\beta_{M+1}|^{L+1}$ with a combination of L -independent model parameters. It picks out the solutions β_M and β_{M+1} of Eq. (7) as the dominant ones at large L , although in this regime, the L dependence is also generally weak since the exponent $1/(L+1)$ changes slowly. Below, we discuss further on the large L and moderate L regimes separately.

In the thermodynamic limit of $L \rightarrow \infty$, the right-hand side of Eq. (16) tends to unity, giving rise to the standard GBZ result $|\beta_M| = |\beta_{M+1}|$ discussed in [87,89,91,110,113,127,137]. Hence, to draw the GBZ for $L \rightarrow \infty$, we uniformly vary the relative phase between β_M and β_{M+1} , and trace out the trajectory \mathcal{C}_β satisfying $|\beta_M| = |\beta_{M+1}|$. Since L is large, each point in the GBZ curve is separated by a $2\pi/L$ phase interval that converges to a continuum, resulting in continuum complex energy bands.

For finite L away from the thermodynamic limit, we emphasize that this standard GBZ construction for $E_\infty = \lim_{L \rightarrow \infty} E_{\text{OBC}}$ may no longer be valid. While in many cases, E_{OBC} does not change significantly as L is extrapolated down to moderate [i.e., $L \sim O(10)$], in cNHSE cases, the spectra and hence other physical properties vary strongly with system size. To characterize such cNHSE scenarios at finite L , we note from Eq. (16) that the magnitudes $|\beta_M|$ and $|\beta_{M+1}|$ can no longer be treated as equal. Physically, this implies that the OBC eigenstates are superpositions of different modes with inverse spatial decay lengths of either $-\ln|\beta_M|$ or $-\ln|\beta_{M+1}|$. As such, the effective cNHSE GBZ is described by *both* $|\beta_M|$ and $|\beta_{M+1}|$, which are no longer equal. Contributions from other β_j solutions affect the eigenstate decay rates negligibly even in the presence of cNHSE, as numerically verified for our illustrative coupled Hatano-Nelson model in Appendix C.

In the following two sections, we shall elaborate on how the pair of GBZ solutions $|\beta_M|$ and $|\beta_{M+1}|$ scale with system size L . Since the exact scaling dependencies can be highly complicated, we shall illustrate our results concretely through two paradigmatic cNHSE models, the minimal cou-

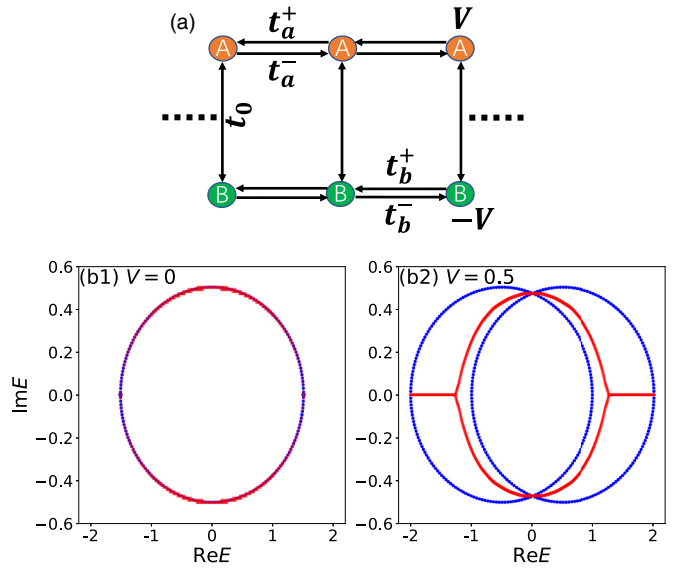


FIG. 1. (a) Coupled Hatano-Nelson chain model [Eq. (18)] with interchain hopping t_0 , intrachain hopping asymmetries $t_a^\pm = t_1 \pm \delta_a$ and $t_b^\pm = t_1 \pm \delta_b$, and chain energy offsets $\pm V$. (b) Energy spectra of Eq. (18) under PBCs (blue) and OBC (red) in the $L \rightarrow \infty$ limit for (b1) $V = 0$ and (b2) $V = 0.5$. Parameters are $t_0 = 0.01$, $t_1 = 0.75$, and $\delta_a = -\delta_b = 0.25$. While the PBC and OBC spectra coincide in the $V = 0$ case studied in [127], they deviate when $V \neq 0$, leading to broken bulk-boundary correspondence.

pled Hatano-Nelson model with energy offset in Sec. III and a model with size-dependent topological states in Sec. IV.

III. COUPLED HATANO-NELSON MODEL WITH ENERGY OFFSET

In this section, we elaborate on a cNHSE model formed by coupling the simplest possible NHSE chains: two equal and oppositely oriented Hatano-Nelson chains. Going beyond the minimal model introduced in Ref. [127], which provided elegant analytic results, we additionally introduce onsite energy offsets $\pm V$ on the two chains, respectively, such that the interchain coupling now also faces nontrivial competition from the energetic separation of $2|V|$. The coupled chains are illustrated in Fig. 1(a), with each chain constituting one of the sublattices A and B. In the basis $\mathbf{C}_\mathbf{k} = (c_{\mathbf{k},A}, c_{\mathbf{k},B})^T$, its momentum-space Hamiltonian is

$$\mathcal{H}(z) = \begin{pmatrix} t_a^+ z + t_a^-/z + V & t_0 \\ t_0 & t_b^+ z + t_b^-/z - V \end{pmatrix}, \quad (17)$$

where $t_a^\pm = t_1 \pm \delta_a$, $t_b^\pm = t_1 \pm \delta_b$, t_0 is the interchain hopping, and $\pm V$ is the onsite potential energy. We denote $z = e^{ik}$ as before, where k is the momentum. It is related via Fourier transformation to the corresponding real-space tight-binding Hamiltonian

$$\begin{aligned} H_r = \sum_n & (t_a^+ c_{n,A}^\dagger c_{n+1,A} + t_a^- c_{n+1,A}^\dagger c_{n,A} + t_0 c_{n,A}^\dagger c_{n,B} \\ & + t_b^+ c_{n,B}^\dagger c_{n+1,B} + t_b^- c_{n+1,B}^\dagger c_{n,B} + t_0 c_{n,B}^\dagger c_{n,A} \\ & + V c_{n,A}^\dagger c_{n,A} - V c_{n,B}^\dagger c_{n,B}), \end{aligned} \quad (18)$$

where $c_{n,\alpha}$ ($c_{n,\alpha}^\dagger$) is the annihilation (creation) operator on site α ($\alpha = A, B$) in unit cell n . Evidently, t_a^+/t_a^- and t_b^+/t_b^- are the hopping asymmetries of chains A and B.

The energy eigenvalues of the Hamiltonian (17) under PBCs are given by

$$E_{\text{PBC}}^{(\pm)}(k) = 2t_1 \cos k + i(\delta_a + \delta_b) \sin k \pm \sqrt{[i(\delta_a - \delta_b) \sin k + V]^2 + t_0^2}, \quad (19)$$

where $k \in \mathbb{R}$ and $t_a^\pm = t_1 \pm \delta_a$, $t_b^\pm = t_1 \pm \delta_b$. In Fig. 1(b1), we see that in the large- L limit, the PBC spectrum (blue) agrees well with the OBC spectrum (red) only in the $V = 0$ case which Ref. [127] has considered. When $V \neq 0$ [Fig. 1(b2)], the OBC spectrum lies in the interior of the PBC loops and can only agree with $E_{\text{PBC}}^{(\pm)}(k)$ if we perform an appropriate complex momentum deformation $k \rightarrow k + i\kappa(k)$ [89,91,99,101,110,113]. While it may appear here that the $V = 0$ case does not experience BBC breaking (i.e., the NHSE), that is actually untrue once we consider finite system sizes [127]. Below, we show that this model exhibits cNHSE at finite system sizes for *all* values of V , and compare some analytic approximations with numerical results.

A. Finite-size scaling from the cNHSE

To understand how the PBC and OBC spectra differ beyond the thermodynamic limit shown in Figs. 1(b1) and 1(b2), we examine the real-space Schrödinger's equation $\mathcal{H}_r|\psi\rangle = E_{\text{OBC}}|\psi\rangle$, where $|\psi\rangle = (\psi_{1,A}, \psi_{1,B}, \psi_{2,A}, \psi_{2,B}, \dots, \psi_{n,A}, \psi_{n,B}, \dots)^T$:

$$\begin{cases} t_a^- \psi_{n-1,A} + t_0 \psi_{n,B} + t_a^+ \psi_{n+1,A} + V \psi_{n,A} = E_{\text{OBC}} \psi_{n,A}, \\ t_b^- \psi_{n-1,B} + t_0 \psi_{n,A} + t_b^+ \psi_{n+1,B} - V \psi_{n,B} = E_{\text{OBC}} \psi_{n,B}, \end{cases} \quad (20)$$

where \mathcal{H}_r is the Hamiltonian matrix of H_r in the basis $(C_1, C_2, \dots, C_j, \dots)^T$. Based on the approach developed in Sec. II, we can use as an eigenstate ansatz which is a linear combination of β solutions, such as to solve the real-space Schrödinger equation [87,112,127]

$$\begin{pmatrix} \psi_{n,A} \\ \psi_{n,B} \end{pmatrix} = \sum_{j=1}^4 (\beta_j)^n \begin{pmatrix} \phi_A^{(j)} \\ \phi_B^{(j)} \end{pmatrix}. \quad (21)$$

This allows us to rewrite Eq. (20) as

$$\begin{pmatrix} t_a^+ \beta + t_a^- \beta^{-1} + V & t_0 \\ t_0 & t_b^+ \beta + t_b^- \beta^{-1} - V \end{pmatrix} \begin{pmatrix} \phi_A \\ \phi_B \end{pmatrix} = E_{\text{OBC}} \begin{pmatrix} \phi_A \\ \phi_B \end{pmatrix}, \quad (22)$$

where we have written $\beta_j = \beta$ and $\phi_\alpha^{(j)} = \phi_\alpha$ ($\alpha = A, B$) for notational simplicity since Eq. (22) applies separately to different j . Essentially, this ansatz has allowed us to replace $z = e^{ik}$ by β . Nontrivial solutions to Eq. (22) satisfy the bulk characteristic dispersion equation

$$\begin{aligned} & t_a^+ t_b^+ \beta^2 - [(t_a^+ + t_b^+) E_{\text{OBC}} + (t_a^+ - t_b^+) V] \beta \\ & + (t_a^+ t_b^- + t_a^- t_b^+ + E_{\text{OBC}}^2 - t_0^2 - V^2) \\ & - [(t_a^- + t_b^-) E_{\text{OBC}} + (t_a^- - t_b^-) V] \beta^{-1} + t_a^- t_b^- \beta^{-2} = 0. \end{aligned} \quad (23)$$

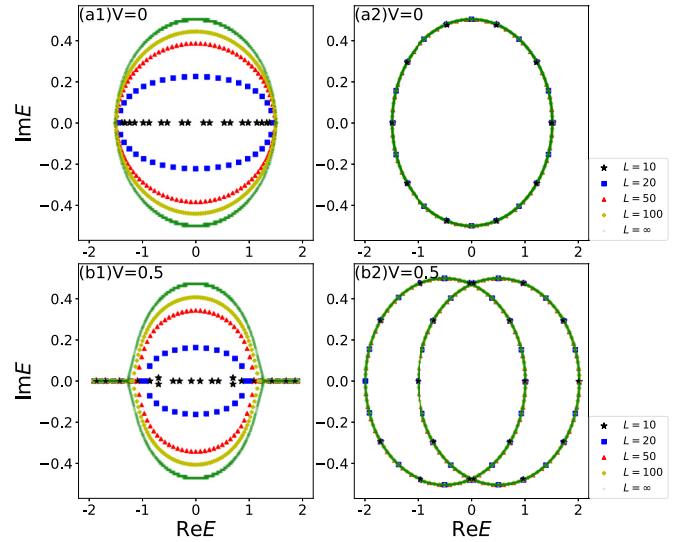


FIG. 2. OBC energy spectra of the coupled Hatano-Nelson model Hamiltonian (18) with (a1) $V = 0$ and (b1) $V = 0.5$ at different finite system sizes $L = 10$ (black), 20 (blue), 50 (red), 100 (yellow), ∞ (green). When $V = 0$, the spectrum is real for short chains, but complex for long chains due to the strong effective couplings from large L . But interestingly for $V \neq 0$, short chains can possess some complex energies, and long chains possess some real energies. PBC energy spectra of the coupled Hatano-Nelson model Hamiltonian (18) with (a2) $V = 0$ and (b2) $V = 0.5$ at different finite system sizes $L = 10$ (black), 20 (blue), 50 (red), 100 (yellow), ∞ (green). Parameters are $t_0 = 0.01$, $t_1 = 0.75$, and $\delta_a = -\delta_b = 0.25$, the same as those in Fig. 1.

For each value of E_{OBC} , there are four solutions $\beta = \beta_j$, $j = 1, 2, 3, 4$, since the maximal and minimal powers of β are $n_+ = n_- = 1$.

1. Finite-size scaling of the OBC spectra

To understand the OBC spectrum E_{OBC} in terms of non-Bloch theory, we need to obtain its effective GBZ. For finite L , the GBZ comprises the two dominant β solutions such that $E_{\text{PBC}}(-i \ln \beta)$ numerically coincides with E_{OBC} . The numerically computed E_{OBC} is shown in Fig. 2 for both (a) $V = 0$ and (b) $V = 0.5$. Evidently, the OBC spectra in both cases depend strongly on L , being real for small L (i.e., $L = 10$), and gradually morphing into the large- L spectrum previously shown in Fig. 1. Physically, the spectrum remains real when the couplings (here with small bare values $t_0 = 0.01$) are strong enough for the directed amplifications from both chains to cancel;² as the system gets larger, the cNHSE becomes exponentially stronger and the couplings serve to “close up” [52,115,138] the amplification loops, causing unchecked amplification that corresponds to complex energies. For $V \neq 0$, some eigenenergies can remain real even at arbitrarily large system sizes presumably because the potential offsets obstruct unchecked amplification.

²Thus directed amplification provides an alternative mechanism for achieving real non-Hermitian spectra [97,139], unrelated to PT symmetry.

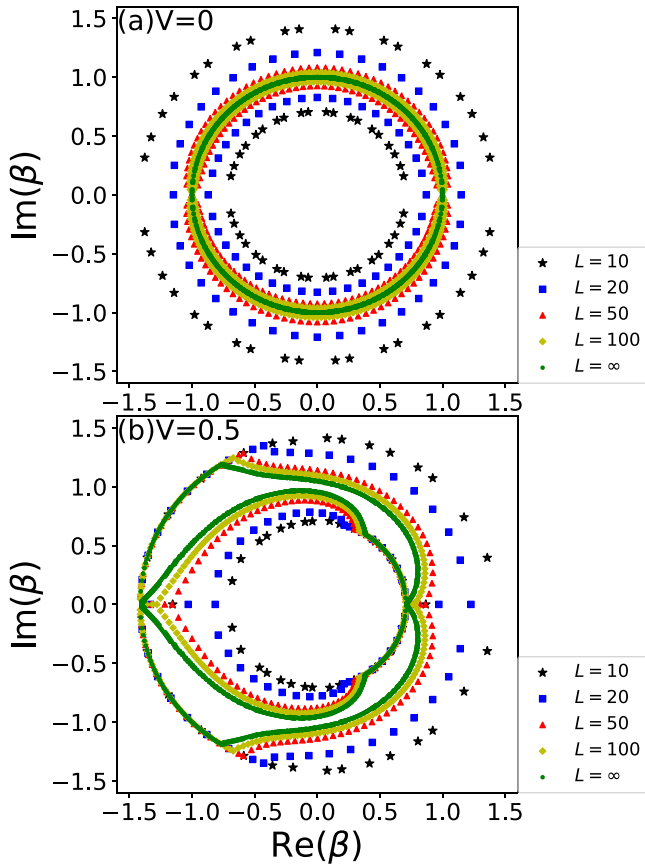


FIG. 3. GBZ of the coupled Hatano-Nelson model Hamiltonian (18) at different finite system sizes $L = 10$ (black), 20 (blue), 50 (red), 100 (yellow), ∞ (green) for (a) $V = 0$ and (b) $V = 0.5$. At finite L , the GBZ is given by solutions $\beta_M = \beta_2$ and $\beta_{M+1} = \beta_3$; as $L \rightarrow \infty$, the β_2 and β_3 loops converge towards the standard GBZ solution $|\beta_2| = |\beta_3|$. Note that this standard GBZ can consist of two loops [as in (b)] since this is a two-band model. Parameters are $t_0 = 0.01$, $t_1 = 0.75$, and $\delta_a = -\delta_b = 0.25$, the same as those in Fig. 1.

2. From OBC spectra to size-dependent cNHSE GBZs

While the size-dependent spectra in Fig. 2 unambiguously signify the presence of cNHSE, size dependencies in the spectra are model specific. Key to more fundamental understanding of cNHSE scaling is the scaling behavior of the GBZ.³ To compute the GBZ, we substitute the OBC energies into the characteristic equation (23) and obtain the β solutions. Here, for each E_{OBC} point, we have four solutions $|\beta_1| \leq |\beta_2| \leq |\beta_3| \leq |\beta_4|$ and the GBZ is given by the two solutions $\beta_M = \beta_2$ and $\beta_{M+1} = \beta_3$. Figure 3 shows the GBZ computed at various finite system sizes $L = 10, 20, 50, 100$; the $L = \infty$ case (green) is plotted by solving Eq. (23) with the standard condition $|\beta_2| = |\beta_3|$ (i.e., intersecting β_2 and β_3 solution curves) [91,106–112] valid in the thermodynamic limit. For the finite-size cases under $V = 0$ shown in Fig. 3(a),

there are two loops in the $\text{Re}(\beta)$ - $\text{Im}(\beta)$ plane for each value of L , corresponding to the β_2 and β_3 solutions. As the system size L increases to infinity, they converge towards each other, as expected from the condition $|\beta_2| = |\beta_3|$. Similarly, for the $V \neq 0$ case in Fig. 3(b), the two loops in the $\text{Re}(\beta)$ - $\text{Im}(\beta)$ plane get closer and closer to each other as the system size L increases. However, in this case, they do not converge into one single loop because the GBZ solution $|\beta_2| = |\beta_3|$ itself consists of two loops [green in Fig. 3(b)]. Here the GBZ solutions are also highly anisotropic in the wave number $\arg(\beta)$, exhibiting cusps at β corresponding to branch points in the spectrum [99,101].

3. Finite scaling behavior of the GBZ

Having numerically seen how the GBZ varies with system size, we now rigorously derive the scaling rules governing it. To do so, we examine the OBC constraints in detail. As elaborated in Appendix D, imposing open boundaries at $x = 1$ and L , i.e., $\psi_{0,\alpha} = \psi_{L+1,\alpha} = 0$ gives rise to the condition

$$\begin{aligned} & X_{1,4}X_{2,3}[(\beta_1\beta_4)^{L+1} + (\beta_2\beta_3)^{L+1}] \\ & - X_{1,3}X_{2,4}[(\beta_1\beta_3)^{L+1} + (\beta_2\beta_4)^{L+1}] \\ & + X_{1,2}X_{3,4}[(\beta_1\beta_2)^{L+1} + (\beta_3\beta_4)^{L+1}] = 0, \end{aligned} \quad (24)$$

where $X_{i,j}$ are defined as

$$X_{i,j} \equiv t_a^+(\beta_j - \beta_i) + t_a^-(\beta_j^{-1} - \beta_i^{-1}) \quad (25)$$

with $i, j = 1, 2, 3, 4$. This result is equivalent to Eq. (8), but specialized to our coupled Hatano-Nelson model Hamiltonian. Interestingly, it is independent of V and E_{OBC} , even though they both definitely affect the values of β_j since the individual β_j solutions are determined by the characteristic dispersion equation (23). When L is varied, the β_j solutions of Eq. (23) vary since E_{OBC} changes with L . How exactly E_{OBC} can change is indirectly constrained by Eq. (24), which imposes a L -dependent relation between the β_j solutions corresponding to the value of E_{OBC} .

To make progress in deriving the finite-size scaling properties of the β s, our strategy is to consider the large- L limit and obtain the leading-order scaling behavior. In this limit, we can approximate the boundary equation (24) by retaining only the two dominant terms $-X_{1,3}X_{2,4}(\beta_2\beta_4)^{L+1}$ and $X_{1,2}X_{3,4}(\beta_3\beta_4)^{L+1}$. To make further headway, we note that the cNHSE is already well manifested when the bare value of the coupling t_0 is very small, i.e., $t_0 = 0.01$ as in Fig. 1. (In fact, if t_0 is of the same order as the two Hatano-Nelson chains, it would be difficult to see the weak coupling/small- L limit with real spectra.) As such, we can expand up to the second order of the coupling parameter t_0 (see Appendix E) to obtain

$$\left| \frac{\beta_2}{\beta_3} \right| \simeq \left| \frac{X_{1,2}X_{3,4}}{X_{1,3}X_{2,4}} \right|^{\frac{1}{L+1}} \approx |(t_a^+ t_b^- - t_a^- t_b^+) f_\infty(E_\infty) t_0^2|^{\frac{1}{L+1}}, \quad (26)$$

where $E_\infty \equiv \lim_{L \rightarrow \infty} E_{\text{OBC}}$, and

$$f_\infty(E_\infty) = \frac{\sqrt{(E_\infty - V)^2 - 4t_a^+ t_a^-} \sqrt{(E_\infty + V)^2 - 4t_b^+ t_b^-}}{h^2(E_\infty)}, \quad (27)$$

³Although the GBZ also depends on the model, at least it remains invariant across models related by conformal transforms in the complex E_{OBC} plane [99,101].

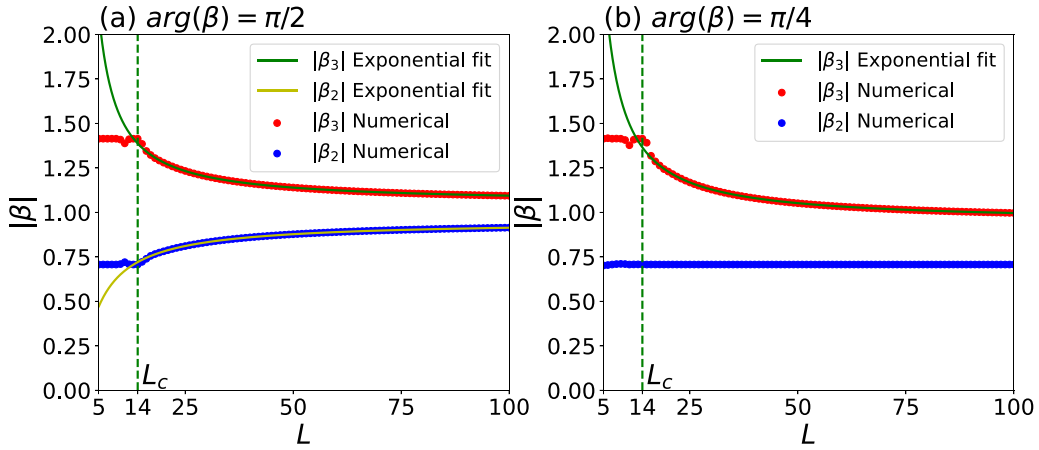


FIG. 4. The GBZ radii $|\beta_2|$ and $|\beta_3|$ of our coupled Hatano-Nelson model Hamiltonian (18) with $V = 0.5$, plotted against the system size L for (a) $\arg(\beta) = \frac{\pi}{2}$ and (b) $\arg(\beta) = \frac{\pi}{4}$. Results obtained from the numerical OBC spectra exhibit excellent fitting with the exponential scaling of Eq. (28), with fitted parameters $a[\arg(\beta) = \frac{\pi}{2}] \approx 0.050$, $b[\arg(\beta) = \frac{\pi}{2}] \approx 78.65$, $a[\arg(\beta) = \frac{\pi}{4}] \approx -0.057$, and $b[\arg(\beta) = \frac{\pi}{4}] \approx 198.11$. The scaling is frozen below the lower critical length $L_c \approx 14$, limited by the bare asymmetric couplings t_a^\pm and t_b^\pm . Parameters are $t_0 = 0.01$, $t_1 = 0.75$, and $\delta_a = -\delta_b = 0.25$, the same as those in Fig. 1.

$h(E_\infty) = E_\infty^2(t_a^- - t_b^-)(t_a^+ - t_b^+) + (t_a^+ t_b^- - t_a^- t_b^+)^2 + 2E_\infty \times (t_a^+ t_a^- - t_b^+ t_b^-)V + (t_a^+ + t_b^+)(t_a^- + t_b^-)V^2$. Notice that E_∞ in Eq. (26) depends on t_0 . Equation (26) is Eq. (16) specialized to our coupled Hatano-Nelson model Hamiltonian [Eq. (18)]. It expresses the ratio of the GBZ quantities $|\beta_2|$ and $|\beta_3|$ as a constant exponentiated by $1/(L+1)$, which is a scaling behavior that is universal across cNHSE models.

While the $1/(L+1)$ exponential scaling behavior holds generally for the ratio $|\beta_M/\beta_{M+1}|$, it can apply to $|\beta_M|$ or $|\beta_{M+1}|$ individually if they are related in special ways. In Fig. 4, we show the numerically extracted $|\beta_2|$ and $|\beta_3|$ at two special values of $\arg(\beta)$, where $|\beta_2| \approx 1/|\beta_3|$ in Fig. 4(a) and $|\beta_2|$ is constant in Fig. 4(b). As such, $|\beta_2/\beta_3| \approx |\beta_2|^2 \approx |\beta_3|^{-2}$ in Fig. 4(a) and $|\beta_2/\beta_3| \propto |\beta_3|^{-1}$ in Fig. 4(b), hence allowing for $|\beta_3|$ to be fitted to an exponential form

$$|\beta_3| = a + bL^{-1}, \quad (28)$$

where the parameters $a, b \in \mathbb{R}$, $b > 0$, and $|a| \ll 1 \ll |b|$. In general, this exponential relation fits the numerically obtained $|\beta|$ s very well for sufficiently large L , as demonstrated in Fig. 4. The actual values of fitting parameters a and b are shown in Fig. 5 as functions of the onsite energy V [Figs. 5(a) and 5(b)] and $\arg(\beta)$ [Figs. 5(c) and 5(d)]. It is found that both a and b are monotonically increasing functions of the onsite energy V at $\arg(\beta) = \frac{\pi}{2}$ [Figs. 5(a) and 5(b)]. Also, in the range of $\arg(\beta) \in [\frac{\pi}{4}, \frac{\pi}{2}]$ for $V = 0.5$, a is a monotonically increasing function of $\arg(\beta)$, but b is a monotonically decreasing function of $\arg(\beta)$. We see that the condition $|a| \ll |b|$ is always satisfied with different onsite energy V and $\arg(\beta)$.

The correctness of our exponential fit can be checked by comparing against analytic results involving the model parameters. From Eq. (26), we see that in the case of $|\beta_2| \approx 1/|\beta_3|$, the parameter b in the exponential scaling relation is approximately given by

$$b \approx |(t_a^+ t_b^- - t_a^- t_b^+)^2 f_\infty(E_\infty) t_0^2|^{-1/2}. \quad (29)$$

As shown in Fig. 5(b), both the analytical and numerical results agree well with each other when the onsite energy V is smaller than 0.2, where the $|\beta_2| \approx 1/|\beta_3|$ approximation accurately holds. For different fixed $\arg(\beta)$, E_{OBC} would be different, leading to different values of b . Indeed, as evident in Fig. 3(b), the convergence behavior of $|\beta|$ and hence b varies significantly with $\arg(\beta)$ [Fig. 5(d)].

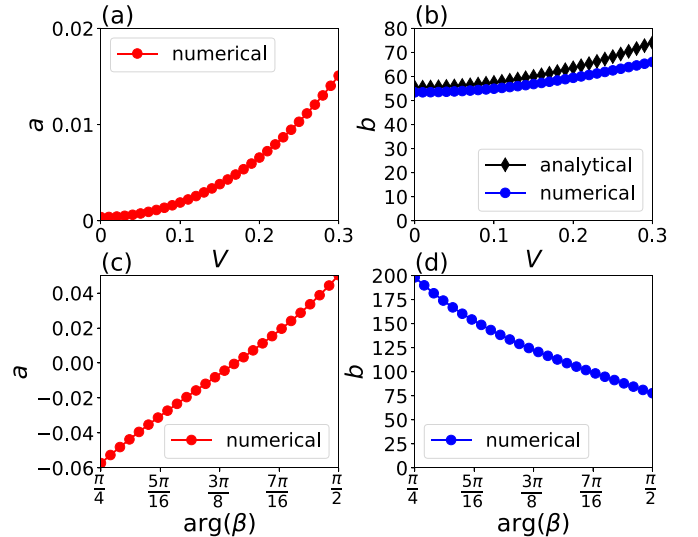


FIG. 5. (a), (b) Exponential scaling parameters a and b [Eq. (28)] of $|\beta_3|$ as a function of V at $\arg(\beta) = \frac{\pi}{2}$. Their numerical values are extracted from the plot of $|\beta_3|$ against L , which is computed from the numerical E_{OBC} data. In (b), this numerically obtained b is shown to be well predicted from the model parameters through the analytic result (29), which is derived under the small- V approximation. (c), (d) Show the numerically obtained a and b as a function of $\arg(\beta)$, at fixed $V = 0.5$. Parameters are $t_0 = 0.01$, $t_1 = 0.75$, and $\delta_a = -\delta_b = 0.25$, the same as those in Fig. 1.

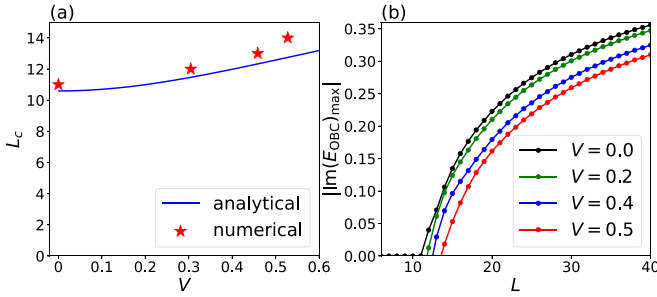


FIG. 6. (a) Critical system size L_c versus V at $\arg(E_{\text{OBC}}) = \frac{\pi}{2}$. The analytical result given by Eq. (30) (blue) agrees reasonably well with numerical results (red stars) estimated by the threshold system size $L = L_c$, below which the spectrum is unaffected by L . We observe that L_c increases with V , confirming the intuition that the interchain energy offset V obstructs critical NHSE hybridization. (b) Absolute value of the maximal imaginary part of the eigenvalues $|\text{Im}(E_{\text{OBC}})_{\text{max}}|$ as a function of the system size L , also at $\arg(E_{\text{OBC}}) = \frac{\pi}{2}$. The onset of complex E_{OBC} typically occurs at L_c , except for small systems ($L = 10$), where the nonzero V offset can give rise to complex energies [see Fig. 2(b)]. Parameters are $t_0 = 0.01$, $t_1 = 0.75$, and $\delta_a = -\delta_b = 0.25$, the same as those in Fig. 1.

B. Lower critical system size for the cNHSE

As seen in Fig. 4, the scaling of the GBZ parameters $|\beta_M|$ and $|\beta_{M+1}|$ ($M = 2$ here) is only exponential and described by Eq. (28) above a certain lower critical system size L_c . Below that, they remain effectively constant, indicative of the absence of the cNHSE. The reason is that the spatial skin decay lengths $-1/\ln|\beta_M|$ and $-1/\ln|\beta_{M+1}|$ cannot be faster than that of the physical NHSE chains in the cNHSE model. In our model, noting that $|\beta_3| > |\beta_2|$, we must have $|\beta_{3c}| = \sqrt{t_a^+/t_a^-}$ and $|\beta_{2c}| = \sqrt{t_b^+/t_b^-}$, corresponding to the $|\beta|$ s of the individual Hatano-Nelson chains.

Substituting $|\beta_2/\beta_3|$ with $|\beta_{2c}/\beta_{3c}|$ in Eq. (26), we obtain the critical system size L_c of our coupled Hatano-Nelson model as

$$L_c \approx \frac{2 \ln |(t_a^+ t_b^- - t_a^- t_b^+)^2 f_\infty(E_\infty) t_0^2|}{\ln |t_b^+ t_a^- / (t_b^- t_a^+)|} - 1. \quad (30)$$

As shown in Fig. 6(a) for $\arg(E_{\text{OBC}}) = \frac{\pi}{2}$, this analytic expression [Eq. (30)] for L_c (blue curve) agrees rather well with its numerical determination (red stars), i.e., from plots such as Fig. 4. Not surprisingly, it increases monotonically with the interchain energy offset V since the offset impedes energy matching and acts as an obstruction to the critical coupling between the Hatano-Nelson chains.

L_c can also be thought of as the lower critical length above which the interchain coupling t_0 is “switched on” to cause the cNHSE. As seen in Fig. 6(b), the energy spectrum becomes complex precisely above L_c . Since our OBC Hatano-Nelson chains have real spectra when uncoupled, it means that they become effective coupled only when $L \geq L_c$. Naively, we would expect small t_0 to continuously give rise to small imaginary energies; yet, in reality, there exists a sharp real-to-complex spectral transition [113,127] controlled by L_c . We note that $L_c \rightarrow \infty$ as $t_0 \rightarrow 0$, consistent with the expectation that uncoupled chains will never experience the cNHSE.

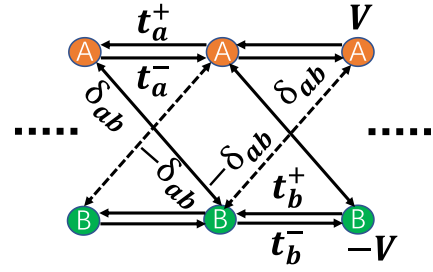


FIG. 7. Topologically coupled two-chain model [Eq. (33)] with crisscrossing interchain nonreciprocal couplings $\pm\delta_{ab}$ and asymmetric hoppings $t_a^\pm = t_1 \pm \delta_a$ and $t_b^\pm = t_1 \pm \delta_b$ in chains A and B. The chains are given energy offsets of $\pm V$.

IV. TOPOLOGICALLY COUPLED CHAIN MODEL

To complement the exposition of our coupled Hatano-Nelson cNHSE model above, we next consider more sophisticated interchain couplings which lead to size-controlled topological states, as first designed in [113]. In the basis $C_{\mathbf{k}} = (c_{\mathbf{k},A}, c_{\mathbf{k},B})^T$, it is given by

$$\mathcal{H}_{\text{top}}(z) = \begin{pmatrix} t_a^+ z + t_a^- / z + V & \delta_{ab}(z + 1/z) \\ -\delta_{ab}(z + 1/z) & t_b^+ z + t_b^- / z - V \end{pmatrix}, \quad (31)$$

where $t_a^\pm = t_1 \pm \delta_a$, $t_b^\pm = t_1 \pm \delta_b$, and $z = e^{ik}$. Here, the simple interchain couplings t_0 of the coupled Hatano-Nelson model are replaced by crisscrossing interchain couplings $\pm\delta_{ab}$ which can potentially introduce topological flux [140]. Under PBCs, the energy eigenvalues can be simply obtained from the Hamiltonian (31) as

$$E_{\text{PBC}}^{(\pm)}(k) = 2t_1 \cos k + i(\delta_a + \delta_b) \sin k \pm \sqrt{[i(\delta_a - \delta_b) \sin k + V]^2 - 4\delta_{ab}^2 \cos^2 k} \quad (32)$$

with $k = -i \ln z \in \mathbb{R}$ and $t_a^\pm = t_1 \pm \delta_a$, $t_b^\pm = t_1 \pm \delta_b$. By Fourier transformation, one obtains the real-space tight-binding Hamiltonian (Fig. 7)

$$\begin{aligned} H_t = & \sum_n (t_a^+ c_{n,A}^\dagger c_{n+1,A} + t_a^- c_{n+1,A}^\dagger c_{n,A} + \delta_{ab} c_{n,A}^\dagger c_{n+1,B} \\ & - \delta_{ab} c_{n+1,B}^\dagger c_{n,A} + t_b^+ c_{n,B}^\dagger c_{n+1,B} + t_b^- c_{n+1,B}^\dagger c_{n,B} \\ & + \delta_{ab} c_{n+1,A}^\dagger c_{n,B} - \delta_{ab} c_{n,B}^\dagger c_{n+1,A} + V c_{n,A}^\dagger c_{n,A} \\ & - V c_{n,B}^\dagger c_{n,B}), \end{aligned} \quad (33)$$

where $c_{n,\alpha}$ ($c_{n,\alpha}^\dagger$) is the annihilation (creation) operator on site α ($\alpha = A, B$) in cell n .

Following the similar derivations as Eq. (23), we can obtain the characteristic energy dispersion equation

$$\begin{aligned} (t_a^+ t_b^+ + \delta_{ab}^2) \beta^2 + [-(t_a^+ + t_b^+) E_{\text{OBC}} - (t_a^+ - t_b^+) V] \beta \\ + (t_a^+ t_b^- + t_a^- t_b^+ + 2\delta_{ab}^2 + E_{\text{OBC}}^2 - V^2) \\ + [-(t_a^- + t_b^-) E_{\text{OBC}} - (t_a^- - t_b^-) V] \beta^{-1} \\ + (t_a^- t_b^- + \delta_{ab}^2) \beta^{-2} = 0. \end{aligned} \quad (34)$$

Similarly as before, we can compute the OBC energy spectra and the GBZ of the topological coupled chain model Hamiltonian (33) at different finite system sizes $L = 10, 30, 50$,

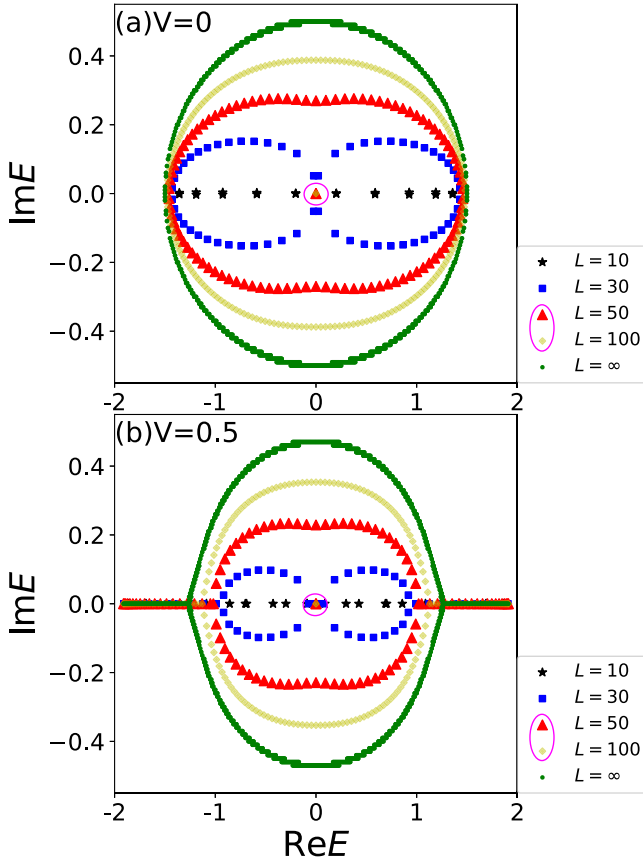


FIG. 8. OBC energy spectra of the topologically coupled chain model Hamiltonian (33) with (a) $V = 0$ and (b) $V = 0.5$ at different system sizes $L = 10$ (black), 30 (blue), 50 (red), 100 (yellow), ∞ (green). Notably, topological zero modes (circled) appear at $E = 0$ in the point gap only at sufficiently large system sizes of $L = 50, 100$. The other parameters are $\delta_{ab} = 0.5 \times 10^{-3}$, $t_1 = 0.75$, and $\delta_a = -\delta_b = 0.25$.

100, ∞ as shown in Figs. 8 and 9, respectively. We find that they are qualitatively similar to those of the coupled Hatano-Nelson model, except that there is a topological zero mode at $E = 0$ (dirty red and yellow). These topological modes also correspond to isolated solutions in the GBZ plot (Fig. 9), although they are exempted from the finite-size scaling behavior. It is found that the topological zero modes appear at $E = 0$ in the point gap only at sufficiently large system sizes as shown in Fig. 8. The reason is that the GBZ depends strongly on the system size as shown in Fig. 9, and so does the OBC spectrum as shown in Fig. 8. When we tune the system size L (regarding L as a parameter), the OBC spectrum changes. At a critical L , the OBC spectrum's gap closes and, after that, topological zero modes appear, as shown in Fig. 13 in Appendix F. Different from the famous single-chain Su-Schrieffer-Heeger model [141–146], our topologically coupled chain model has two coupled chains, i.e., the coupling between these two chains plays an important role here. In the topologically coupled chain model, the competition between the coupling of the two chains and the finite system size determines the existence or absence of the topological zero modes. This conclusion can be found by calculating the topological phase diagram of the

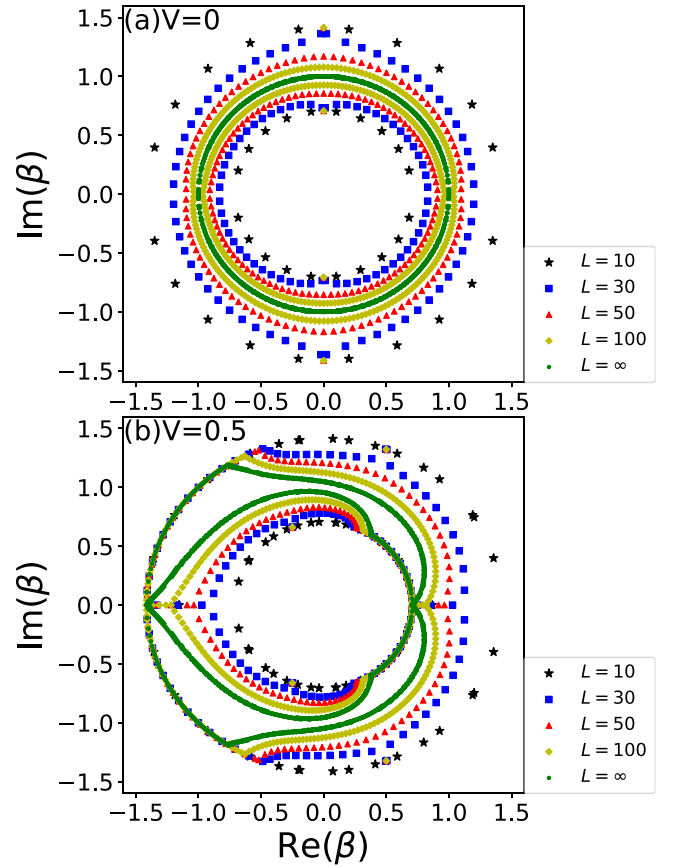


FIG. 9. GBZ of the topologically coupled chain model Hamiltonian (33) at different finite system sizes $L = 10$ (black), 20 (blue), 50 (red), 100 (yellow), ∞ (green) with (a) $V = 0$ and (b) $V = 0.5$. Parameters are $\delta_{ab} = 0.5 \times 10^{-3}$, $t_1 = 0.75$, and $\delta_a = -\delta_b = 0.25$, the same as those in Fig. 8. The GBZ is qualitatively similar to that in Fig. 3, apart from the isolated topological modes (dirty red and yellow) which by definition do not belong to any continuum of states.

topologically coupled chain model as shown in Fig. 4(d) in a previous work [113]. Therefore, the strength of the coupling of the two chains determines the threshold system size which is required for the topological modes.

By enforcing OBCs in the real-space Hamiltonian, we arrive at

$$\begin{aligned} & [Z_{1,4}^{(b)} Z_{2,3}^{(a)} (\beta_1 \beta_4)^{L+1} + Z_{1,4}^{(a)} Z_{2,3}^{(b)} (\beta_2 \beta_3)^{L+1}] \\ & - [Z_{1,3}^{(b)} Z_{2,4}^{(a)} (\beta_1 \beta_3)^{L+1} + Z_{1,3}^{(a)} Z_{2,4}^{(b)} (\beta_2 \beta_4)^{L+1}] \\ & + [Z_{1,2}^{(b)} Z_{3,4}^{(a)} (\beta_1 \beta_2)^{L+1} + Z_{1,2}^{(a)} Z_{3,4}^{(b)} (\beta_3 \beta_4)^{L+1}] = 0, \end{aligned} \quad (35)$$

where dispersion relation solutions β_j ($j = 1, 2, 3, 4$) are arranged so that $|\beta_1| \leq |\beta_2| \leq |\beta_3| \leq |\beta_4|$, and $Z_{i,j}^{(c)}$ ($i, j = 1, 2, 3, 4$; $c = a, b$) are defined as

$$Z_{i,j}^{(c)} = X_i^{(c)} Y_j^{(c)} - X_j^{(c)} Y_i^{(c)}. \quad (36)$$

Here, $X_j^{(c)}$ and $Y_j^{(c)}$ are defined as

$$X_j^{(a)} = E_{\text{OBC}} - (t_a^+ - t_a^-) \beta_j - V, \quad (37)$$

$$Y_j^{(a)} = E_{\text{OBC}} - (t_b^+ - t_b^-) \beta_j + V, \quad (38)$$

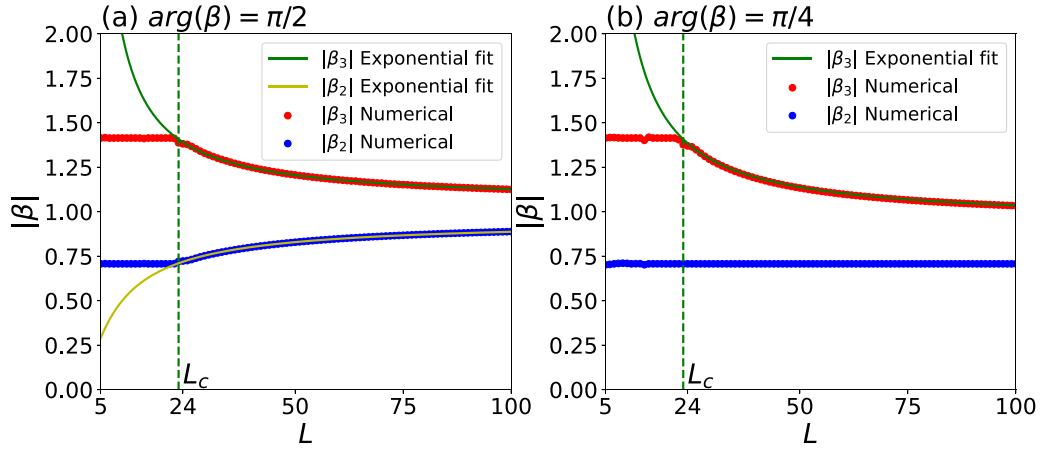


FIG. 10. The GBZ radii $|\beta_2|$ and $|\beta_3|$ of the topologically coupled chain model Hamiltonian (33) versus the system size L at (a) $\arg(\beta) = \frac{\pi}{2}$ and (b) $\arg(\beta) = \frac{\pi}{4}$. The exponential fits of $|\beta_3|$ correspond to scaling parameters $a[\arg(\beta) = \frac{\pi}{2}] \approx 0.0520$, $b[\arg(\beta) = \frac{\pi}{2}] \approx 1476.563$, $a[\arg(\beta) = \frac{\pi}{4}] \approx -0.0607$, and $b[\arg(\beta) = \frac{\pi}{4}] \approx 8791.616$. The cNHSE scaling is frozen below $L = L_c \approx 23$, but at $\arg(\beta) = \frac{\pi}{4}$, $|\beta_2|$ remains constant across all L . Here, $V = 0.5$ and the other parameters $\delta_{ab} = 0.5 \times 10^{-3}$, $t_1 = 0.75$, and $\delta_a = -\delta_b = 0.25$ are the same as those in Fig. 9.

$$X_j^{(b)} = E_{\text{OBC}} + (t_a^+ - t_a^-)\beta_j^{-1} - V, \quad (39)$$

$$Y_j^{(b)} = E_{\text{OBC}} + (t_b^+ - t_b^-)\beta_j^{-1} + V. \quad (40)$$

The corresponding derivation of Eq. (35) is given in Appendix G.

To deal with Eq. (35), we only consider the two dominant terms $-Z_{1,3}^{(a)}Z_{2,4}^{(b)}(\beta_2\beta_4)^{L+1}$ and $Z_{1,2}^{(a)}Z_{3,4}^{(b)}(\beta_3\beta_4)^{L+1}$ on the left-hand side. In this case, by substituting the solutions of the characteristic equation (34) into this approximated boundary equation, we can approximate Eq. (35) as

$$\left| \frac{\beta_2}{\beta_3} \right| \approx \left| \frac{Z_{1,2}^{(a)}Z_{3,4}^{(b)}}{Z_{1,3}^{(a)}Z_{2,4}^{(b)}} \right|_{E_{\text{OBC}}=E_\infty}^{\frac{1}{L+1}} \approx \left| \frac{\Delta_a(E_\infty - V + \Delta_a)\Delta_b(E_\infty + V + \Delta_b)}{2t_a^+t_b^- [V^2 - E_\infty^2 + 2(t_a^+t_b^- + t_b^+t_a^-) + \Delta_a\Delta_b]} \right|^{\frac{1}{L+1}}, \quad (41)$$

where $\Delta_a = \sqrt{(E_\infty - V)^2 - 4t_a^+t_a^-}$, $\Delta_b = \sqrt{(E_\infty + V)^2 - 4t_b^+t_b^-}$, and we have used the approximation $\delta_{ab} \rightarrow 0$ under the condition of weak interchain couplings. Notice that E_∞ in Eq. (41) depends on δ_{ab} . Therefore, we can also follow Eq. (28) and postulate an exponential fitting ansatz of $|\beta_3|$ as

$$|\beta_3| = a + bL^{\frac{1}{L+1}}, \quad (42)$$

for cases where $|\beta_2| \approx 1/|\beta_3|$. The scaling behavior of a and b in Eq. (42) can be extracted or estimated from the asymptotic result (41) with the model parameters.

In Figs. 10(a) and 10(b), we show $|\beta_2|$ and $|\beta_3|$ for the topologically coupled chain model Hamiltonian (33) as a function of the system size L both from the exponential formula in Eq. (42) and from numerical diagonalization. We observe an exponential scaling behavior qualitatively similar to that of the coupled Hatano-Nelson model, which should also universally hold for other cNHSE models.

V. ROBUST SPECTRAL SCALING BEHAVIOR UNDER DISORDER

In this section, we check the robustness of the scaling behavior of the OBC spectra in the presence of uniformly distributed onsite disorder

$$H_{\text{dis}} = \sum_{n,\alpha} \tilde{w}(n, \alpha) c_{n,\alpha}^\dagger c_{n,\alpha} \quad (43)$$

with random number $\tilde{w} \in [-w/2, w/2]$ and $\alpha = A, B$ are the site indices in the cell n . Since the GBZ is directly determined through the OBC spectrum, robustness in the scaling behavior in the spectrum would also imply similar robustness in the GBZ.

In Fig. 11, we plot the absolute value of the maximal imaginary part of the eigenenergies $|\text{Im}(E_{\text{OBC}})_{\text{max}}|$ as a

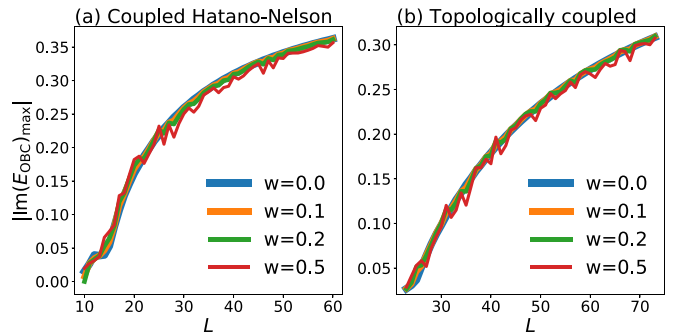


FIG. 11. Absolute value of the maximal imaginary part of the eigenvalues $|\text{Im}(E_{\text{OBC}})_{\text{max}}|$ for different system sizes L , which is satisfied for the eigenenergy with $\arg(E_{\text{OBC}}) = \frac{\pi}{2}$. In both (a) the coupled Hatano-Nelson model [Eq. (18)] and (b) the topologically coupled chain model [Eq. (33)], the spectral scaling behavior is very robust up to disorder strength $w = 0.2$, as defined in Eq. (43). Even at much larger disorder $w = 0.5$, the same qualitative spectral scaling prevails. Here, $V = 0.5$ and the other parameters are $t_0 = 0.01$, $\delta_{ab} = 0.5 \times 10^{-3}$, $t_1 = 0.75$, and $\delta_a = -\delta_b = 0.25$, the same as those in previous figures on these respective models.

function of the system size L under different disorder strengths from $w = 0$ to 0.5 . $|\text{Im}(E_{\text{OBC}})_{\text{max}}|$ determines the “width” of the spectrum in the imaginary direction and can be used as a measure of how the shape of the spectrum is deformed under disorder. For our models, $|\text{Im}(E_{\text{OBC}})_{\text{max}}|$ usually occurs when $\arg(E_{\text{OBC}}) = \frac{\pi}{2}$, but that is not necessarily universal. From Fig. 11, we find that relatively weak disorder ($w < 0.2$) affects the spectrum negligibly, but moderately large disorder ($w = 0.5$) gives rise to visible spectral perturbations. However, the qualitative spectral scaling behavior remains very robust, which indicates that the cNHSE is strongly robust against onsite disorder. This is not surprising given that the cNHSE arises from the competition between different NHSE channels, and should not be affected too much by the onsite energy landscape. It has to be noted that *hopping* disorder, however, can affect the long-time state dynamics and hence significantly modify the overall energy spectrum [126,147–150].

VI. DISCUSSION

Systems experiencing the critical non-Hermitian skin effect (cNHSE) are particularly sensitive to the system size, exhibiting qualitatively different spectra and spatial eigenstate behavior at different sizes L . How the cNHSE scaling is exactly described by the GBZ, particularly for a system of finite size, is an open question. As we already know, the GBZ can be used to restore the BBC in the thermodynamic limit. But for a system of finite size, can GBZ still be a valid theoretical framework? Using the GBZ as a tool to investigate

the cNHSE scaling behavior provides an effective way to understand the physical picture of the finite-size effect on the competing NHSE tendencies between small and large size limits.

In this work, we considered a generic two-component cNHSE ansatz model with two competing NHSE channels, and provided detailed studies of two paradigmatic models, of which the minimal model studied by Ref. [127] is a special case. We find that our effective finite-size GBZ obeys a universal exponential scaling law, with exponent inversely proportional to the system size, and scaling rate b expressible in term of the model parameters in certain cases. Based on this, we provide detailed and empirically verified estimates of the critical system size L_c where such a scaling relation begins to hold both analytically and numerically.

Such cNHSE phenomena can be readily experimentally demonstrated in non-Hermitian metamaterials with well-controlled gain and loss and effective couplings, such as photonic crystal arrays and electrical circuits. Since the nonreciprocity from different NHSE can cancel, the setup may not even require physical asymmetric couplings, such as in the recent experiment [52]. Moving forward, it would be immensely interesting to explore the interplay of cNHSE and many-body interactions in emerging and rapidly progressing platforms such as ultracold atomic arrays and quantum circuits.

ACKNOWLEDGMENTS

We thank Zhesen Yang, Kai Zhang, and Chen Fang for helpful discussions. F.Q. is supported by the Singapore National Research Foundation (Grant No. NRF2021-QEP2-02-P09).

APPENDIX A: DERIVATION OF THE DETERMINANT FORM OF THE OBC CONSTRAINTS FOR A TWO-BAND cNHSE MODEL [EQ. (8)]

From the bulk eigenequation in Eq. (6), we obtain

$$\begin{cases} \left[\sum_{n=-n_-}^{n_+} h_n^{aa}(\beta_j)^n - E_{\text{OBC}} \right] \phi_A^{(j)} + \sum_{n=-n_-}^{n_+} h_n^{ab}(\beta_j)^n \phi_B^{(j)} = 0, & \frac{\phi_B^{(j)}}{\phi_A^{(j)}} = \frac{E_{\text{OBC}} - \sum_{n=-n_-}^{n_+} h_n^{aa}(\beta_j)^n}{\sum_{n=-n_-}^{n_+} h_n^{ab}(\beta_j)^n}, \\ \sum_{n=-n_-}^{n_+} h_n^{ba}(\beta_j)^n \phi_A^{(j)} + \left[\sum_{n=-n_-}^{n_+} h_n^{bb}(\beta_j)^n - E_{\text{OBC}} \right] \phi_B^{(j)} = 0, & \frac{\phi_B^{(j)}}{\phi_A^{(j)}} = \frac{\sum_{n=-n_-}^{n_+} h_n^{ba}(\beta_j)^n}{E_{\text{OBC}} - \sum_{n=-n_-}^{n_+} h_n^{bb}(\beta_j)^n}, \end{cases} \quad (\text{A1})$$

i.e.,

$$\frac{\phi_B^{(j)}}{\phi_A^{(j)}} = \frac{E_{\text{OBC}} - \sum_{n=-n_-}^{n_+} h_n^{aa}(\beta_j)^n}{\sum_{n=-n_-}^{n_+} h_n^{ab}(\beta_j)^n} = \frac{\sum_{n=-n_-}^{n_+} h_n^{ba}(\beta_j)^n}{E_{\text{OBC}} - \sum_{n=-n_-}^{n_+} h_n^{bb}(\beta_j)^n} = f_j, \quad (\text{A2})$$

$$\begin{bmatrix} \sum_{n=-n_-}^{n_+} h_n^{ab}(\beta_j)^n \end{bmatrix} \begin{bmatrix} \sum_{n=-n_-}^{n_+} h_n^{ba}(\beta_j)^n \end{bmatrix} = \begin{bmatrix} E_{\text{OBC}} - \sum_{n=-n_-}^{n_+} h_n^{aa}(\beta_j)^n \end{bmatrix} \begin{bmatrix} E_{\text{OBC}} - \sum_{n=-n_-}^{n_+} h_n^{bb}(\beta_j)^n \end{bmatrix}, \quad (\text{A3})$$

$$\phi_B^{(j)} = f_j \phi_A^{(j)}, \quad (\text{A4})$$

which also relates E_{OBC} with β_j solutions.

Substituting these real-space eigenequations under the OBC constraints $\psi_{-n_-, \alpha} = \dots = \psi_{-1, \alpha} = \psi_{0, \alpha} = \psi_{L+1, \alpha} = \psi_{L+2, \alpha} = \dots = \psi_{L+n_+, \alpha} = 0$ ($\alpha = \text{A, B}$; $1 \leq n_{\pm} \leq L/2$) into the real-space Schrödinger equation $\mathcal{H}_{gr}|\psi\rangle = E_{\text{OBC}}|\psi\rangle$ [where \mathcal{H}_{gr} is the

Hamiltonian matrix of H_{gr} in the basis $(C_1, C_2, \dots, C_L)^T$, we can get

$$\left\{ \begin{array}{l}
 \sum_{n=0}^{n_+} h_n^{aa} \psi_{1+n,A} + \sum_{n=0}^{n_+} h_n^{ab} \psi_{1+n,B} = E_{\text{OBC}} \psi_{1,A}, \\
 \sum_{n=0}^{n_+} h_n^{ba} \psi_{1+n,A} + \sum_{n=0}^{n_+} h_n^{bb} \psi_{1+n,B} = E_{\text{OBC}} \psi_{1,B}, \\
 \sum_{n=-1}^{n_+} h_n^{aa} \psi_{2+n,A} + \sum_{n=-1}^{n_+} h_n^{ab} \psi_{2+n,B} = E_{\text{OBC}} \psi_{2,A}, \\
 \sum_{n=-1}^{n_+} h_n^{ba} \psi_{2+n,A} + \sum_{n=-1}^{n_+} h_n^{bb} \psi_{2+n,B} = E_{\text{OBC}} \psi_{2,B}, \\
 \vdots \\
 \sum_{n=-(n_+-1)}^{n_+} h_n^{aa} \psi_{n_++n,A} + \sum_{n=-(n_+-1)}^{n_+} h_n^{ab} \psi_{n_++n,B} = E_{\text{OBC}} \psi_{n_+,A}, \quad 1 \leq 2n_+ \leq L, \quad 1 \leq n_+ \leq L/2 \\
 \sum_{n=-(n_+-1)}^{n_+} h_n^{ba} \psi_{n_++n,A} + \sum_{n=-(n_+-1)}^{n_+} h_n^{bb} \psi_{n_++n,B} = E_{\text{OBC}} \psi_{n_+,B}, \quad 1 \leq 2n_+ \leq L, \quad 1 \leq n_+ \leq L/2 \\
 \sum_{n=-n_-}^{n_-1} h_n^{aa} \psi_{L-(n_-1)+n,A} + \sum_{n=-n_-}^{n_-1} h_n^{ab} \psi_{L-(n_-1)+n,B} = E_{\text{OBC}} \psi_{L-(n_-1),A}, \quad 1 \leq L-2n_-+1 \leq L \\
 \sum_{n=-n_-}^{n_-1} h_n^{ba} \psi_{L-(n_-1)+n,A} + \sum_{n=-n_-}^{n_-1} h_n^{bb} \psi_{L-(n_-1)+n,B} = E_{\text{OBC}} \psi_{L-(n_-1),B}, \quad 1 \leq n_- \leq L/2 \\
 \vdots \\
 \sum_{n=-n_-}^1 h_n^{aa} \psi_{L-1+n,A} + \sum_{n=-n_-}^1 h_n^{ab} \psi_{L-1+n,B} = E_{\text{OBC}} \psi_{L-1,A}, \\
 \sum_{n=-n_-}^1 h_n^{ba} \psi_{L-1+n,A} + \sum_{n=-n_-}^1 h_n^{bb} \psi_{L-1+n,B} = E_{\text{OBC}} \psi_{L-1,B}, \\
 \sum_{n=-n_-}^0 h_n^{aa} \psi_{L+n,A} + \sum_{n=-n_-}^0 h_n^{ab} \psi_{L+n,B} = E_{\text{OBC}} \psi_{L,A}, \quad 1 \leq L-n_- \leq L, \quad 0 \leq n_- \leq L-1 \\
 \sum_{n=-n_-}^0 h_n^{ba} \psi_{L+n,A} + \sum_{n=-n_-}^0 h_n^{bb} \psi_{L+n,B} = E_{\text{OBC}} \psi_{L,B}, \quad 1 \leq L-n_- \leq L, \quad 0 \leq n_- \leq L-1.
 \end{array} \right. \tag{A5}$$

Invoking the non-Bloch ansatz $(\psi_{n,A}, \psi_{n,B})^T = \sum_{j=1}^{2M} (\beta_j)^n (\phi_A^{(j)}, \phi_B^{(j)})^T$ ($M = n_- + n_+$) into the above equations (A5), we have, generalizing [89],

$$\left\{ \begin{array}{l}
 \sum_{j=1}^{2M} \sum_{n=0}^{n_+} h_n^{aa} (\beta_j)^{1+n} \phi_A^{(j)} + \sum_{j=1}^{2M} \sum_{n=0}^{n_+} h_n^{ab} (\beta_j)^{1+n} \phi_B^{(j)} = E_{\text{OBC}} \sum_{j=1}^{2M} (\beta_j) \phi_A^{(j)}, \\
 \sum_{j=1}^{2M} \sum_{n=0}^{n_+} h_n^{ba} (\beta_j)^{1+n} \phi_A^{(j)} + \sum_{j=1}^{2M} \sum_{n=0}^{n_+} h_n^{bb} (\beta_j)^{1+n} \phi_B^{(j)} = E_{\text{OBC}} \sum_{j=1}^{2M} (\beta_j) \phi_B^{(j)}, \\
 \sum_{j=1}^{2M} \sum_{n=-1}^{n_+} h_n^{aa} (\beta_j)^{2+n} \phi_A^{(j)} + \sum_{j=1}^{2M} \sum_{n=-1}^{n_+} h_n^{ab} (\beta_j)^{2+n} \phi_B^{(j)} = E_{\text{OBC}} \sum_{j=1}^{2M} (\beta_j)^2 \phi_A^{(j)}, \\
 \sum_{j=1}^{2M} \sum_{n=-1}^{n_+} h_n^{ba} (\beta_j)^{2+n} \phi_A^{(j)} + \sum_{j=1}^{2M} \sum_{n=-1}^{n_+} h_n^{bb} (\beta_j)^{2+n} \phi_B^{(j)} = E_{\text{OBC}} \sum_{j=1}^{2M} (\beta_j)^2 \phi_B^{(j)}, \\
 \vdots \\
 \sum_{j=1}^{2M} \sum_{n=-(n_+-1)}^{n_+} h_n^{aa} (\beta_j)^{n_++n} \phi_A^{(j)} + \sum_{j=1}^{2M} \sum_{n=-(n_+-1)}^{n_+} h_n^{ab} (\beta_j)^{n_++n} \phi_B^{(j)} = E_{\text{OBC}} \sum_{j=1}^{2M} (\beta_j)^{n_+} \phi_A^{(j)}, \\
 \sum_{j=1}^{2M} \sum_{n=-(n_+-1)}^{n_+} h_n^{ba} (\beta_j)^{n_++n} \phi_A^{(j)} + \sum_{j=1}^{2M} \sum_{n=-(n_+-1)}^{n_+} h_n^{bb} (\beta_j)^{n_++n} \phi_B^{(j)} = E_{\text{OBC}} \sum_{j=1}^{2M} (\beta_j)^{n_+} \phi_B^{(j)}, \\
 \sum_{j=1}^{2M} \sum_{n=-n_-}^{n_+-1} h_n^{aa} (\beta_j)^{L-(n_+-1)+n} \phi_A^{(j)} + \sum_{j=1}^{2M} \sum_{n=-n_-}^{n_+-1} h_n^{ab} (\beta_j)^{L-(n_+-1)+n} \phi_B^{(j)} = E_{\text{OBC}} \sum_{j=1}^{2M} (\beta_j)^{L-(n_+-1)} \phi_A^{(j)}, \\
 \sum_{j=1}^{2M} \sum_{n=-n_-}^{n_+-1} h_n^{ba} (\beta_j)^{L-(n_+-1)+n} \phi_A^{(j)} + \sum_{j=1}^{2M} \sum_{n=-n_-}^{n_+-1} h_n^{bb} (\beta_j)^{L-(n_+-1)+n} \phi_B^{(j)} = E_{\text{OBC}} \sum_{j=1}^{2M} (\beta_j)^{L-(n_+-1)} \phi_B^{(j)}, \\
 \vdots \\
 \sum_{j=1}^{2M} \sum_{n=-n_-}^1 h_n^{aa} (\beta_j)^{L-1+n} \phi_A^{(j)} + \sum_{j=1}^{2M} \sum_{n=-n_-}^1 h_n^{ab} (\beta_j)^{L-1+n} \phi_B^{(j)} = E_{\text{OBC}} \sum_{j=1}^{2M} (\beta_j)^{L-1} \phi_A^{(j)}, \\
 \sum_{j=1}^{2M} \sum_{n=-n_-}^1 h_n^{ba} (\beta_j)^{L-1+n} \phi_A^{(j)} + \sum_{j=1}^{2M} \sum_{n=-n_-}^1 h_n^{bb} (\beta_j)^{L-1+n} \phi_B^{(j)} = E_{\text{OBC}} \sum_{j=1}^{2M} (\beta_j)^{L-1} \phi_B^{(j)}, \\
 \sum_{j=1}^{2M} \sum_{n=-n_-}^0 h_n^{aa} (\beta_j)^{L+n} \phi_A^{(j)} + \sum_{j=1}^{2M} \sum_{n=-n_-}^0 h_n^{ab} (\beta_j)^{L+n} \phi_B^{(j)} = E_{\text{OBC}} \sum_{j=1}^{2M} (\beta_j)^L \phi_A^{(j)}, \\
 \sum_{j=1}^{2M} \sum_{n=-n_-}^0 h_n^{ba} (\beta_j)^{L+n} \phi_A^{(j)} + \sum_{j=1}^{2M} \sum_{n=-n_-}^0 h_n^{bb} (\beta_j)^{L+n} \phi_B^{(j)} = E_{\text{OBC}} \sum_{j=1}^{2M} (\beta_j)^L \phi_B^{(j)}.
 \end{array} \right. \tag{A6}$$

Substituting Eq. (A4), i.e., $\phi_B^{(j)} = f_j \phi_A^{(j)}$, into the above equations (A6) such as to eliminate the $\phi_B^{(j)}$, we have

$$\left(\begin{array}{l}
 \sum_{j=1}^{2M} \left[\sum_{n=0}^{n_+} (h_n^{aa} + f_j h_n^{ab})(\beta_j)^n - E_{\text{OBC}} \right] (\beta_j) \phi_A^{(j)} = 0, \\
 \sum_{j=1}^{2M} \left[\sum_{n=0}^{n_+} (h_n^{ba} + f_j h_n^{bb})(\beta_j)^n - f_j E_{\text{OBC}} \right] (\beta_j) \phi_A^{(j)} = 0, \\
 \sum_{j=1}^{2M} \left[\sum_{n=-1}^{n_+} (h_n^{aa} + f_j h_n^{ab})(\beta_j)^n - E_{\text{OBC}} \right] (\beta_j)^2 \phi_A^{(j)} = 0, \\
 \sum_{j=1}^{2M} \left[\sum_{n=-1}^{n_+} (h_n^{ba} + f_j h_n^{bb})(\beta_j)^n - f_j E_{\text{OBC}} \right] (\beta_j)^2 \phi_A^{(j)} = 0, \\
 \vdots \\
 \sum_{j=1}^{2M} \left[\sum_{n=-(n_+-1)}^{n_+} (h_n^{aa} + f_j h_n^{ab})(\beta_j)^n - E_{\text{OBC}} \right] (\beta_j)^{n_+} \phi_A^{(j)} = 0, \\
 \sum_{j=1}^{2M} \left[\sum_{n=-(n_+-1)}^{n_+} (h_n^{ba} + f_j h_n^{bb})(\beta_j)^n - f_j E_{\text{OBC}} \right] (\beta_j)^{n_+} \phi_A^{(j)} = 0, \\
 \sum_{j=1}^{2M} \left[\sum_{n=-n_-}^{n_-1} (h_n^{aa} + f_j h_n^{ab})(\beta_j)^n - E_{\text{OBC}} \right] (\beta_j)^{L-(n_-1)} \phi_A^{(j)} = 0, \\
 \sum_{j=1}^{2M} \left[\sum_{n=-n_-}^{n_-1} (h_n^{ba} + f_j h_n^{bb})(\beta_j)^n - f_j E_{\text{OBC}} \right] (\beta_j)^{L-(n_-1)} \phi_A^{(j)} = 0, \\
 \vdots \\
 \sum_{j=1}^{2M} \left[\sum_{n=-n_-}^1 (h_n^{aa} + f_j h_n^{ab})(\beta_j)^n - E_{\text{OBC}} \right] (\beta_j)^{L-1} \phi_A^{(j)} = 0, \\
 \sum_{j=1}^{2M} \left[\sum_{n=-n_-}^1 (h_n^{ba} + f_j h_n^{bb})(\beta_j)^n - f_j E_{\text{OBC}} \right] (\beta_j)^{L-1} \phi_A^{(j)} = 0, \\
 \sum_{j=1}^{2M} \left[\sum_{n=-n_-}^0 (h_n^{aa} + f_j h_n^{ab})(\beta_j)^n - E_{\text{OBC}} \right] (\beta_j)^L \phi_A^{(j)} = 0, \\
 \sum_{j=1}^{2M} \left[\sum_{n=-n_-}^0 (h_n^{ba} + f_j h_n^{bb})(\beta_j)^n - f_j E_{\text{OBC}} \right] (\beta_j)^L \phi_A^{(j)} = 0.
 \end{array} \right. \quad (\text{A7})$$

We can express Eq. (A7) in more compact notation

$$\left\{ \begin{array}{l}
 \sum_{j=1}^{2M} F_j^{(a,1)} \beta_j \phi_A^{(j)} = 0, \\
 \sum_{j=1}^{2M} F_j^{(b,1)} \beta_j \phi_A^{(j)} = 0, \\
 \vdots \\
 \sum_{j=1}^{2M} F_j^{(a,n_+)} (\beta_j)^{n_+} \phi_A^{(j)} = 0, \\
 \sum_{j=1}^{2M} F_j^{(b,n_+)} (\beta_j)^{n_+} \phi_A^{(j)} = 0, \\
 \sum_{j=1}^{2M} G_j^{(a,1)} (\beta_j)^{L-(n-1)} \phi_A^{(j)} = 0, \\
 \sum_{j=1}^{2M} G_j^{(b,1)} (\beta_j)^{L-(n-1)} \phi_A^{(j)} = 0, \\
 \vdots \\
 \sum_{j=1}^{2M} G_j^{(a,n_-)} (\beta_j)^L \phi_A^{(j)} = 0, \\
 \sum_{j=1}^{2M} G_j^{(b,n_-)} (\beta_j)^L \phi_A^{(j)} = 0,
 \end{array} \right. \quad (\text{A8})$$

where

$$F_j^{(a,i)} = \sum_{n=-(i-1)}^{n_+} (h_n^{aa} + f_j h_n^{ab}) (\beta_j)^n - E_{\text{OBC}}, \quad (\text{A9})$$

$$F_j^{(b,i)} = \sum_{n=-(i-1)}^{n_+} (h_n^{ba} + f_j h_n^{bb}) (\beta_j)^n - f_j E_{\text{OBC}}, \quad (\text{A10})$$

$$G_j^{(a,i)} = \sum_{n=-n_-}^{n_- - i} (h_n^{aa} + f_j h_n^{ab}) (\beta_j)^n - E_{\text{OBC}}, \quad (\text{A11})$$

$$G_j^{(b,i)} = \sum_{n=-n_-}^{n_- - i} (h_n^{ba} + f_j h_n^{bb}) (\beta_j)^n - f_j E_{\text{OBC}}. \quad (\text{A12})$$

For a nontrivial state $\phi_A^{(j)}$ ($j = 1, 2, \dots, 2M$) that does not vanish, we hence require the vanishing determinant

$$\begin{vmatrix}
 F_1^{(a,1)} \beta_1 & F_2^{(a,1)} \beta_2 & \cdots & F_{2M}^{(a,1)} \beta_{2M} \\
 F_1^{(b,1)} \beta_1 & F_2^{(b,1)} \beta_2 & \cdots & F_{2M}^{(b,1)} \beta_{2M} \\
 \vdots & \vdots & \vdots & \vdots \\
 F_1^{(a,n_+)} (\beta_1)^{n_+} & F_2^{(a,n_+)} (\beta_2)^{n_+} & \cdots & F_{2M}^{(a,n_+)} (\beta_{2M})^{n_+} \\
 F_1^{(b,n_+)} (\beta_1)^{n_+} & F_2^{(b,n_+)} (\beta_2)^{n_+} & \cdots & F_{2M}^{(b,n_+)} (\beta_{2M})^{n_+} \\
 G_1^{(a,1)} (\beta_1)^{L-(n-1)} & G_2^{(a,1)} (\beta_2)^{L-(n-1)} & \cdots & G_{2M}^{(a,1)} (\beta_{2M})^{L-(n-1)} \\
 G_1^{(b,1)} (\beta_1)^{L-(n-1)} & G_2^{(b,1)} (\beta_2)^{L-(n-1)} & \cdots & G_{2M}^{(b,1)} (\beta_{2M})^{L-(n-1)} \\
 \vdots & \vdots & \vdots & \vdots \\
 G_1^{(a,n_-)} (\beta_1)^L & G_2^{(a,n_-)} (\beta_2)^L & \cdots & G_{2M}^{(a,n_-)} (\beta_{2M})^L \\
 G_1^{(b,n_-)} (\beta_1)^L & G_2^{(b,n_-)} (\beta_2)^L & \cdots & G_{2M}^{(b,n_-)} (\beta_{2M})^L
 \end{vmatrix} = 0. \quad (\text{A13})$$

**APPENDIX B: DERIVATION OF THE DETERMINANT FORM OF THE OBC CONSTRAINTS
FOR A GENERAL MULTIBAND MODEL**

Here, we generalize the above derivation to a general multiband model, and show that the OBC constraints result in an analogous vanishing determinant expression. In momentum space, an N -band model Hamiltonian in the basis $C_{\mathbf{k}} = (c_{\mathbf{k},1}, c_{\mathbf{k},2}, \dots, c_{\mathbf{k},N})^T$ is given by

$$\mathcal{H}_{mb}(z) = \sum_{n=-n_-}^{n_+} \begin{pmatrix} h_n^{11} & h_n^{12} & \dots & h_n^{1N} \\ h_n^{21} & h_n^{22} & \dots & h_n^{2N} \\ \vdots & \vdots & \ddots & \vdots \\ h_n^{N1} & h_n^{N2} & \dots & h_n^{NN} \end{pmatrix} z^n, \quad (\text{B1})$$

where N is the number of bands, which we set to be an even number.

By Fourier transformation, one obtains the real-space tight-binding Hamiltonian of this system as

$$H_{mbr} = \sum_{j=1}^L \sum_{n=-n_-}^{n_+} C_j^\dagger \begin{pmatrix} h_n^{11} & h_n^{12} & \dots & h_n^{1N} \\ h_n^{21} & h_n^{22} & \dots & h_n^{2N} \\ \vdots & \vdots & \ddots & \vdots \\ h_n^{N1} & h_n^{N2} & \dots & h_n^{NN} \end{pmatrix} C_{j+n}, \quad (\text{B2})$$

where $C_j = (c_{j,1}, c_{j,2}, \dots, c_{j,N})^T$.

With $|\psi\rangle = (\psi_{1,1}, \psi_{1,2}, \dots, \psi_{1,N}, \psi_{2,1}, \psi_{2,2}, \dots, \psi_{2,N}, \dots, \psi_{L,1}, \psi_{L,2}, \dots, \psi_{L,N})^T$, the solutions of the real-space Schrödinger equation $\mathcal{H}_{mbr}|\psi\rangle = E_{\text{OBC}}|\psi\rangle$ [where \mathcal{H}_{mbr} is the Hamiltonian matrix of H_{mbr} in the basis $(C_1, C_2, \dots, C_L)^T$] can be given by

$$\begin{pmatrix} \psi_{n,1} \\ \psi_{n,2} \\ \vdots \\ \psi_{n,N} \end{pmatrix} = \sum_{j=1}^{2M} (\beta_j)^n \begin{pmatrix} \phi_1^{(j)} \\ \phi_2^{(j)} \\ \vdots \\ \phi_N^{(j)} \end{pmatrix}, \quad (\text{B3})$$

where $2M = N \times (n_- + n_+)$ and $\beta = \beta_j$ are the solutions of the characteristic equation

$$\text{Det}[\mathcal{H}_{mb}(\beta) - E_{\text{OBC}}] = 0, \quad (\text{B4})$$

where $\mathcal{H}_{mb}(\beta)$ is the non-Bloch matrix [127] as

$$\mathcal{H}_{mb}(\beta) = \sum_{n=-n_-}^{n_+} \begin{pmatrix} h_n^{11} & h_n^{12} & \dots & h_n^{1N} \\ h_n^{21} & h_n^{22} & \dots & h_n^{2N} \\ \vdots & \vdots & \ddots & \vdots \\ h_n^{N1} & h_n^{N2} & \dots & h_n^{NN} \end{pmatrix} \beta^n. \quad (\text{B5})$$

In general, the characteristic equation (B4) has $2M$ solutions for β , where $M = N \times (n_- + n_+)/2$ is an integer and N is an even number. We label these solutions such that $|\beta_1| \leq |\beta_2| \leq \dots \leq |\beta_{2M}|$.

From the eigenequations, we obtain

$$\begin{cases} \sum_{n=-n_-}^{n_+} h_n^{11} (\beta_j)^n \phi_1^{(j)} + \sum_{n=-n_-}^{n_+} h_n^{12} (\beta_j)^n \phi_2^{(j)} + \dots + \sum_{n=-n_-}^{n_+} h_n^{1N} (\beta_j)^n \phi_N^{(j)} = E_{\text{OBC}} \phi_1^{(j)}, \\ \sum_{n=-n_-}^{n_+} h_n^{21} (\beta_j)^n \phi_1^{(j)} + \sum_{n=-n_-}^{n_+} h_n^{22} (\beta_j)^n \phi_2^{(j)} + \dots + \sum_{n=-n_-}^{n_+} h_n^{2N} (\beta_j)^n \phi_N^{(j)} = E_{\text{OBC}} \phi_2^{(j)}, \\ \vdots \\ \sum_{n=-n_-}^{n_+} h_n^{N1} (\beta_j)^n \phi_1^{(j)} + \sum_{n=-n_-}^{n_+} h_n^{N2} (\beta_j)^n \phi_2^{(j)} + \dots + \sum_{n=-n_-}^{n_+} h_n^{NN} (\beta_j)^n \phi_N^{(j)} = E_{\text{OBC}} \phi_N^{(j)}, \end{cases} \quad (\text{B6})$$

i.e.,

$$\left\{ \begin{array}{l} \left[\sum_{n=-n_-}^{n_+} h_n^{11}(\beta_j)^n - E_{\text{OBC}} \right] \phi_1^{(j)} + \sum_{n=-n_-}^{n_+} h_n^{12}(\beta_j)^n \phi_2^{(j)} + \cdots + \sum_{n=-n_-}^{n_+} h_n^{1N}(\beta_j)^n \phi_N^{(j)} = 0, \\ \sum_{n=-n_-}^{n_+} h_n^{21}(\beta_j)^n \phi_1^{(j)} + \left[\sum_{n=-n_-}^{n_+} h_n^{22}(\beta_j)^n - E_{\text{OBC}} \right] \phi_2^{(j)} + \cdots + \sum_{n=-n_-}^{n_+} h_n^{2N}(\beta_j)^n \phi_N^{(j)} = 0, \\ \vdots \\ \sum_{n=-n_-}^{n_+} h_n^{N1}(\beta_j)^n \phi_1^{(j)} + \sum_{n=-n_-}^{n_+} h_n^{N2}(\beta_j)^n \phi_2^{(j)} + \cdots + \left[\sum_{n=-n_-}^{n_+} h_n^{NN}(\beta_j)^n - E_{\text{OBC}} \right] \phi_N^{(j)} = 0, \end{array} \right. \quad (\text{B7})$$

i.e.,

$$\left\{ \begin{array}{l} \left[\sum_{n=-n_-}^{n_+} h_n^{11}(\beta_j)^n - E_{\text{OBC}} \right] \phi_1^{(j)} + \sum_{n=-n_-}^{n_+} h_n^{12}(\beta_j)^n f_j^{(2)} \phi_1^{(j)} + \cdots + \sum_{n=-n_-}^{n_+} h_n^{1N}(\beta_j)^n f_j^{(N)} \phi_1^{(j)} = 0, \\ \sum_{n=-n_-}^{n_+} h_n^{21}(\beta_j)^n \phi_1^{(j)} + \left[\sum_{n=-n_-}^{n_+} h_n^{22}(\beta_j)^n - E_{\text{OBC}} \right] f_j^{(2)} \phi_1^{(j)} + \cdots + \sum_{n=-n_-}^{n_+} h_n^{2N}(\beta_j)^n f_j^{(N)} \phi_1^{(j)} = 0, \\ \vdots \\ \sum_{n=-n_-}^{n_+} h_n^{N1}(\beta_j)^n \phi_1^{(j)} + \sum_{n=-n_-}^{n_+} h_n^{N2}(\beta_j)^n f_j^{(2)} \phi_1^{(j)} + \cdots + \left[\sum_{n=-n_-}^{n_+} h_n^{NN}(\beta_j)^n - E_{\text{OBC}} \right] f_j^{(N)} \phi_1^{(j)} = 0, \end{array} \right. \quad (\text{B8})$$

where $f_j^{(\alpha)} = \phi_\alpha^{(j)} / \phi_1^{(j)}$ with $\alpha = 1, 2, \dots, N$, i.e.,

$$\phi_\alpha^{(j)} = f_j^{(\alpha)} \phi_1^{(j)}, \quad (\text{B9})$$

where $\alpha = 1, 2, \dots, N$.

As we know, Eq. (B3) has $2M \times N$ unknown coefficients, but with the real-space Schrödinger equation $\mathcal{H}_{mbr}|\psi\rangle = E_{\text{OBC}}|\psi\rangle$ and an additional $2M$ boundary conditions, the $2M \times N$ coefficients can be reduced to $2M$ -independent coefficients. By rewriting the coupling constraints in terms of $\phi_1^{(j)}$ ($j = 1, 2, \dots, 2M$), which should have nonzero values, we have, analogously as before,

$$\left| \begin{array}{cccc} \tilde{F}_1^{(1,1)} \beta_1 & \tilde{F}_2^{(1,1)} \beta_2 & \cdots & \tilde{F}_{2M}^{(1,1)} \beta_{2M} \\ \tilde{F}_1^{(2,1)} \beta_1 & \tilde{F}_2^{(2,1)} \beta_2 & \cdots & \tilde{F}_{2M}^{(2,1)} \beta_{2M} \\ \vdots & \vdots & \vdots & \vdots \\ \tilde{F}_1^{(N,1)} \beta_1 & \tilde{F}_2^{(N,1)} \beta_2 & \cdots & \tilde{F}_{2M}^{(N,1)} \beta_{2M} \\ \vdots & \vdots & \vdots & \vdots \\ \tilde{F}_1^{(1,n_+)} (\beta_1)^{n_+} & \tilde{F}_2^{(1,n_+)} (\beta_2)^{n_+} & \cdots & \tilde{F}_{2M}^{(1,n_+)} (\beta_{2M})^{n_+} \\ \tilde{F}_1^{(2,n_+)} (\beta_1)^{n_+} & \tilde{F}_2^{(2,n_+)} (\beta_2)^{n_+} & \cdots & \tilde{F}_{2M}^{(2,n_+)} (\beta_{2M})^{n_+} \\ \vdots & \vdots & \vdots & \vdots \\ \tilde{F}_1^{(N,n_+)} (\beta_1)^{n_+} & \tilde{F}_2^{(N,n_+)} (\beta_2)^{n_+} & \cdots & \tilde{F}_{2M}^{(N,n_+)} (\beta_{2M})^{n_+} \\ \tilde{G}_1^{(1,1)} (\beta_1)^{L-(n-1)} & \tilde{G}_2^{(1,1)} (\beta_2)^{L-(n-1)} & \cdots & \tilde{G}_{2M}^{(1,1)} (\beta_{2M})^{L-(n-1)} \\ \tilde{G}_1^{(2,1)} (\beta_1)^{L-(n-1)} & \tilde{G}_2^{(2,1)} (\beta_2)^{L-(n-1)} & \cdots & \tilde{G}_{2M}^{(2,1)} (\beta_{2M})^{L-(n-1)} \\ \vdots & \vdots & \vdots & \vdots \\ \tilde{G}_1^{(N,1)} (\beta_1)^{L-(n-1)} & \tilde{G}_2^{(N,1)} (\beta_2)^{L-(n-1)} & \cdots & \tilde{G}_{2M}^{(N,1)} (\beta_{2M})^{L-(n-1)} \\ \vdots & \vdots & \vdots & \vdots \\ \tilde{G}_1^{(1,n_-)} (\beta_1)^L & \tilde{G}_2^{(1,n_-)} (\beta_2)^L & \cdots & \tilde{G}_{2M}^{(1,n_-)} (\beta_{2M})^L \\ \tilde{G}_1^{(2,n_-)} (\beta_1)^L & \tilde{G}_2^{(2,n_-)} (\beta_2)^L & \cdots & \tilde{G}_{2M}^{(2,n_-)} (\beta_{2M})^L \\ \vdots & \vdots & \vdots & \vdots \\ \tilde{G}_1^{(N,n_-)} (\beta_1)^L & \tilde{G}_2^{(N,n_-)} (\beta_2)^L & \cdots & \tilde{G}_{2M}^{(N,n_-)} (\beta_{2M})^L \end{array} \right| = 0, \quad (\text{B10})$$

where

$$\tilde{F}_j^{(1,i)} = \sum_{n=-(i-1)}^{n_+} (h_n^{11} + f_j^{(2)} h_n^{12} + \cdots + f_j^{(N)} h_n^{1N}) (\beta_j)^n - E_{\text{OBC}}, \quad (\text{B11})$$

$$\tilde{F}_j^{(2,i)} = \sum_{n=-(i-1)}^{n_+} (h_n^{21} + f_j^{(2)} h_n^{22} + \cdots + f_j^{(N)} h_n^{2N}) (\beta_j)^n - f_j^{(2)} E_{\text{OBC}}, \quad (\text{B12})$$

⋮

$$\tilde{F}_j^{(N,i)} = \sum_{n=-(i-1)}^{n_+} (h_n^{N1} + f_j^{(2)} h_n^{N2} + \cdots + f_j^{(N)} h_n^{NN}) (\beta_j)^n - f_j^{(N)} E_{\text{OBC}}, \quad (\text{B13})$$

$$\tilde{G}_j^{(1,i)} = \sum_{n=-n_-}^{n_- - i} (h_n^{11} + f_j^{(2)} h_n^{12} + \cdots + f_j^{(N)} h_n^{1N}) (\beta_j)^n - E_{\text{OBC}}, \quad (\text{B14})$$

$$\tilde{G}_j^{(2,i)} = \sum_{n=-n_-}^{n_- - i} (h_n^{12} + f_j^{(2)} h_n^{22} + \cdots + f_j^{(N)} h_n^{2N}) (\beta_j)^n - f_j^{(2)} E_{\text{OBC}}, \quad (\text{B15})$$

⋮

$$\tilde{G}_j^{(N,i)} = \sum_{n=-n_-}^{n_- - i} (h_n^{N1} + f_j^{(2)} h_n^{N2} + \cdots + f_j^{(N)} h_n^{NN}) (\beta_j)^n - f_j^{(N)} E_{\text{OBC}}. \quad (\text{B16})$$

We can collect the terms and express Eq. (B10) as a multivariate polynomial of the form

$$\sum_{P,Q} \tilde{J}(\beta_{i \in P}, \beta_{j \in Q}, E_{\text{OBC}}) \left[\prod_{i \in P} (\beta_i)^k \right] \left[\prod_{j \in Q} (\beta_j)^{k'} \right] = 0, \quad (\text{B17})$$

where $k = 1, \dots, n_+$, $k' = L - (n_- - 1), \dots, L$, the sets P and Q are two disjoint subsets of the set $\{1, 2, \dots, 2M\}$ with M elements, respectively.

By setting $n_+ = n_-$, Eq. (B17) can be reduced to

$$\sum_{P,Q} \tilde{J}(\beta_{i \in P}, \beta_{j \in Q}, E_{\text{OBC}}) \left[\prod_{i \in P} (\beta_i)^{L+1} \right] = 0. \quad (\text{B18})$$

In Eq. (B18), there are two leading terms proportional to $(\beta_M \beta_{M+2} \beta_{M+3} \dots \beta_{2M})^{L+1}$ and $(\beta_{M+1} \beta_{M+2} \beta_{M+3} \dots \beta_{2M})^{L+1}$. Therefore, in the limit of large system size L , we can reduce (B18), which solves the characteristic dispersion equation (B4) and open boundary conditions, to the familiar form

$$\left| \frac{\beta_M}{\beta_{M+1}} \right| \simeq \left| - \frac{\tilde{J}(\beta_{i \in P_1}, \beta_{j \in Q_1}, E_{\text{OBC}})}{\tilde{J}(\beta_{i \in P_2}, \beta_{j \in Q_2}, E_{\text{OBC}})} \right|_{E_{\text{OBC}}=E_\infty}^{\frac{1}{L+1}}, \quad (\text{B19})$$

where $P_1 = \{M+1, M+2, M+3, \dots, 2M\}$, $Q_1 = \{1, 2, 3, \dots, M\}$, $P_2 = \{M, M+2, M+3, \dots, 2M\}$, $Q_2 = \{1, 2, \dots, M-2, M-1, M+1\}$, and L is the system size with $L \rightarrow \infty$. For large L , the right-hand side tends towards unity, and hence $|\beta_M| \approx |\beta_{M+1}|$ for the OBC eigenfunctions in the thermodynamic limit (in practice, $L \simeq 20$ is usually sufficient large when the cNHSE is *absent*).

APPENDIX C: NUMERICAL CONFIRMATION OF THE VALIDITY OF THE GBZ UPON EXTRAPOLATING TO FINITE-SIZE SYSTEMS

Here in Fig. 12, we numerically confirm that for our coupled Hatano-Nelson model, the GBZ solutions $\beta_M = \beta_2$ and $\beta_{M+1} = \beta_3$ still largely determine the eigensolution decay rates down to small system sizes.

APPENDIX D: DERIVATION OF EQ. (24) FOR THE OBC CONSTRAINTS OF THE COUPLED HATANO-NELSON MODEL

From the real-space eigenequations (20) subjected to OBCs $\psi_{0,\alpha} = \psi_{L+1,\alpha} = 0$ ($\alpha = \text{A, B}$), we have

$$\begin{cases} t_0 \psi_{1,\text{B}} + t_a^+ \psi_{2,\text{A}} + V \psi_{1,\text{A}} = E_{\text{OBC}} \psi_{1,\text{A}}, \\ t_0 \psi_{1,\text{A}} + t_b^+ \psi_{2,\text{B}} - V \psi_{1,\text{B}} = E_{\text{OBC}} \psi_{1,\text{B}}, \\ t_a^- \psi_{L-1,\text{A}} + t_0 \psi_{L,\text{B}} + V \psi_{L,\text{A}} = E_{\text{OBC}} \psi_{L,\text{A}}, \\ t_b^- \psi_{L-1,\text{B}} + t_0 \psi_{L,\text{A}} - V \psi_{L,\text{B}} = E_{\text{OBC}} \psi_{L,\text{B}}. \end{cases} \quad (\text{D1})$$

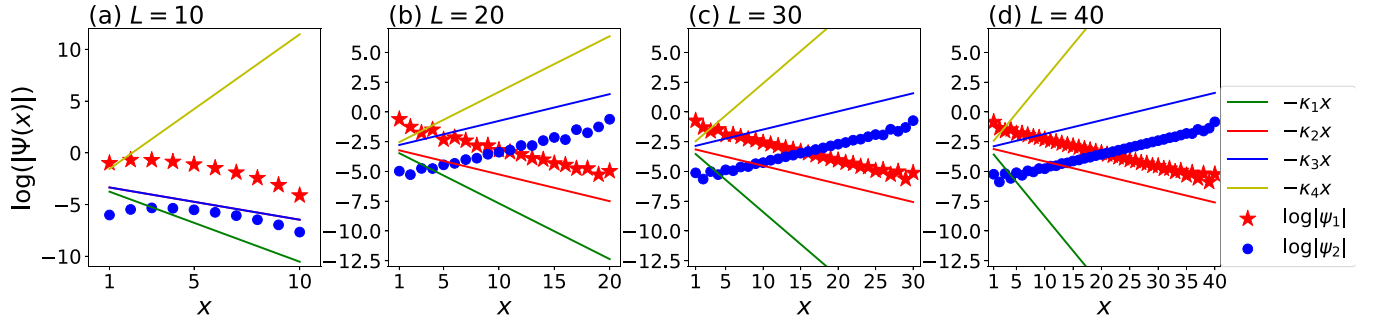


FIG. 12. Spatial decay of eigenstates and how they are determined by β_M and β_{M+1} ($M = 2$). Plotted are the $\ln[|\psi(x)|]$ of two representative eigenstates with different left and right localizations (red stars and blue disks), at different finite system sizes $L = 10, 20, 30, 40$ (a)–(d). Compared against them are the decay profiles corresponding to the four $\kappa = -\ln|\beta|$ solutions. We see that $|\beta_2| = e^{-\kappa_2}$ and $|\beta_3| = e^{-\kappa_3}$ controls the eigenstate decay rate very well down to $L = 20$, even though, in principle, they rigorously determine the decay rate only in the thermodynamic limit. (a) The eigenstates correspond to $\arg(E_{\text{OBC}}) = 0$ and $\text{Max}[\text{Re}(E_{\text{OBC}})]$. (b)–(d) The eigenstates correspond to $\arg(E_{\text{OBC}}) = \frac{\pi}{2}$. Here, $V = 0.5$ and the other parameters are $t_0 = 0.01$, $t_1 = 0.75$, and $\delta_a = -\delta_b = 0.25$, which are the same as those in Fig. 1 of the main text.

By substituting the ansatz $(\psi_{n,A}, \psi_{n,B})^T = \sum_{j=1}^4 \beta_j^n (\phi_A^{(j)}, \phi_B^{(j)})^T$ into Eq. (D1), we can get

$$\begin{cases} t_0 \sum_{j=1}^4 \beta_j \phi_B^{(j)} + t_a^+ \sum_{j=1}^4 \beta_j^2 \phi_A^{(j)} + V \sum_{j=1}^4 \beta_j \phi_A^{(j)} = E_{\text{OBC}} \sum_{j=1}^4 \beta_j \phi_A^{(j)}, \\ t_0 \sum_{j=1}^4 \beta_j \phi_A^{(j)} + t_b^+ \sum_{j=1}^4 \beta_j^2 \phi_B^{(j)} - V \sum_{j=1}^4 \beta_j \phi_B^{(j)} = E_{\text{OBC}} \sum_{j=1}^4 \beta_j \phi_B^{(j)}, \\ t_a^- \sum_{j=1}^4 \beta_j^{L-1} \phi_A^{(j)} + t_0 \sum_{j=1}^4 \beta_j^L \phi_B^{(j)} + V \sum_{j=1}^4 \beta_j^L \phi_A^{(j)} = E_{\text{OBC}} \sum_{j=1}^4 \beta_j^L \phi_A^{(j)}, \\ t_b^- \sum_{j=1}^4 \beta_j^{L-1} \phi_B^{(j)} + t_0 \sum_{j=1}^4 \beta_j^L \phi_A^{(j)} - V \sum_{j=1}^4 \beta_j^L \phi_B^{(j)} = E_{\text{OBC}} \sum_{j=1}^4 \beta_j^L \phi_B^{(j)}. \end{cases} \quad (\text{D2})$$

Furthermore, by using the bulk eigenequation in Eq. (22),

$$\begin{cases} (t_a^+ \beta + t_a^- \beta^{-1} + V - E_{\text{OBC}}) \phi_A + t_0 \phi_B = 0, & \frac{\phi_B}{\phi_A} = -\frac{(t_a^+ \beta + t_a^- \beta^{-1} + V - E_{\text{OBC}})}{t_0}, \\ t_0 \phi_A + (t_b^+ \beta + t_b^- \beta^{-1} - V - E_{\text{OBC}}) \phi_B = 0, & \frac{\phi_B}{\phi_A} = -\frac{t_0}{(t_b^+ \beta + t_b^- \beta^{-1} - V - E_{\text{OBC}})}, \end{cases} \quad (\text{D3})$$

i.e.,

$$\frac{\phi_B^{(j)}}{\phi_A^{(j)}} = \frac{(E_{\text{OBC}} - t_a^+ \beta_j - t_a^- \beta_j^{-1} - V)}{t_0} = \frac{t_0}{(E_{\text{OBC}} - t_b^+ \beta_j - t_b^- \beta_j^{-1} + V)} = f_j, \quad (\text{D4})$$

$$t_0^2 = (E_{\text{OBC}} - t_a^+ \beta_j - t_a^- \beta_j^{-1} - V)(E_{\text{OBC}} - t_b^+ \beta_j - t_b^- \beta_j^{-1} + V), \quad (\text{D5})$$

$$\phi_B^{(j)} = f_j \phi_A^{(j)}, \quad (\text{D6})$$

we have

$$\begin{cases} t_0 \sum_{j=1}^4 \beta_j f_j \phi_A^{(j)} + t_a^+ \sum_{j=1}^4 \beta_j^2 \phi_A^{(j)} + V \sum_{j=1}^4 \beta_j \phi_A^{(j)} = E_{\text{OBC}} \sum_{j=1}^4 \beta_j \phi_A^{(j)}, \\ t_0 \sum_{j=1}^4 \beta_j \phi_A^{(j)} + t_b^+ \sum_{j=1}^4 \beta_j^2 f_j \phi_A^{(j)} - V \sum_{j=1}^4 \beta_j f_j \phi_A^{(j)} = E_{\text{OBC}} \sum_{j=1}^4 \beta_j f_j \phi_A^{(j)}, \\ t_a^- \sum_{j=1}^4 \beta_j^{L-1} \phi_A^{(j)} + t_0 \sum_{j=1}^4 \beta_j^L f_j \phi_A^{(j)} + V \sum_{j=1}^4 \beta_j^L \phi_A^{(j)} = E_{\text{OBC}} \sum_{j=1}^4 \beta_j^L \phi_A^{(j)}, \\ t_b^- \sum_{j=1}^4 \beta_j^{L-1} f_j \phi_A^{(j)} + t_0 \sum_{j=1}^4 \beta_j^L \phi_A^{(j)} - V \sum_{j=1}^4 \beta_j^L f_j \phi_A^{(j)} = E_{\text{OBC}} \sum_{j=1}^4 \beta_j^L f_j \phi_A^{(j)}, \end{cases} \quad (\text{D7})$$

$$\left\{ \begin{aligned} & \sum_{j=1}^4 (E_{\text{OBC}} - t_a^+ \beta_j - t_a^- \beta_j^{-1} - V) \beta_j \phi_A^{(j)} + t_a^+ \sum_{j=1}^4 \beta_j^2 \phi_A^{(j)} + V \sum_{j=1}^4 \beta_j \phi_A^{(j)} = E_{\text{OBC}} \sum_{j=1}^4 \beta_j \phi_A^{(j)}, \\ & t_0 \sum_{j=1}^4 \beta_j \phi_A^{(j)} + \sum_{j=1}^4 (t_b^+ \beta_j - V - E_{\text{OBC}}) \beta_j f_j \phi_A^{(j)} = 0, \\ & t_a^- \sum_{j=1}^4 \beta_j^{L-1} \phi_A^{(j)} + \sum_{j=1}^4 (E_{\text{OBC}} - t_a^+ \beta_j - t_a^- \beta_j^{-1} - V) \beta_j^L \phi_A^{(j)} + V \sum_{j=1}^4 \beta_j^L \phi_A^{(j)} = E_{\text{OBC}} \sum_{j=1}^4 \beta_j^L \phi_A^{(j)}, \\ & \sum_{j=1}^4 (t_b^- \beta_j^{-1} - V - E_{\text{OBC}}) \beta_j^L f_j \phi_A^{(j)} + t_0 \sum_{j=1}^4 \beta_j^L \phi_A^{(j)} = 0, \end{aligned} \right. \quad (\text{D8})$$

$$\left\{ \begin{aligned} & \sum_{j=1}^4 (-t_a^- \beta_j^{-1}) \beta_j \phi_A^{(j)} = 0, \\ & \sum_{j=1}^4 \beta_j \phi_A^{(j)} + \sum_{j=1}^4 \frac{(t_b^+ \beta_j - V - E_{\text{OBC}})}{(E_{\text{OBC}} - t_b^+ \beta_j - t_b^- \beta_j^{-1} + V)} \beta_j \phi_A^{(j)} = 0, \\ & \sum_{j=1}^4 (-t_a^+ \beta_j) \beta_j^L \phi_A^{(j)} = 0, \\ & \sum_{j=1}^4 \frac{(t_b^- \beta_j^{-1} - V - E_{\text{OBC}})}{(E_{\text{OBC}} - t_b^+ \beta_j - t_b^- \beta_j^{-1} + V)} \beta_j^L \phi_A^{(j)} + \sum_{j=1}^4 \beta_j^L \phi_A^{(j)} = 0, \end{aligned} \right. \quad (\text{D9})$$

$$\left\{ \begin{aligned} & \sum_{j=1}^4 \phi_A^{(j)} = 0, \\ & \sum_{j=1}^4 \frac{1}{(E_{\text{OBC}} - t_b^+ \beta_j - t_b^- \beta_j^{-1} + V)} \phi_A^{(j)} = 0, \quad \sum_{j=1}^4 \phi_A^{(j)} = \sum_{j=1}^4 (E_{\text{OBC}} - t_a^+ \beta_j - t_a^- \beta_j^{-1} - V) \phi_A^{(j)} = 0, \\ & \sum_{j=1}^4 \beta_j^{L+1} \phi_A^{(j)} = 0, \\ & \sum_{j=1}^4 \frac{1}{(E_{\text{OBC}} - t_b^+ \beta_j - t_b^- \beta_j^{-1} + V)} \beta_j^{L+1} \phi_A^{(j)} = 0, \quad \sum_{j=1}^4 (E_{\text{OBC}} - t_a^+ \beta_j - t_a^- \beta_j^{-1} - V) \beta_j^{L+1} \phi_A^{(j)} = 0, \end{aligned} \right. \quad (\text{D10})$$

where we have used the characteristic dispersion equation

$$\frac{1}{(E_{\text{OBC}} - t_b^+ \beta_j - t_b^- \beta_j^{-1} + V)} = \frac{(E_{\text{OBC}} - t_a^+ \beta_j - t_a^- \beta_j^{-1} - V)}{t_0^2}. \quad (\text{D11})$$

Imposing the condition that $\phi_A^{(j)}$ ($j = 1, 2, 3, 4$) do not vanish, we must have the vanishing determinant:

$$\begin{vmatrix} 1 & 1 & 1 & 1 \\ X_1 & X_2 & X_3 & X_4 \\ \beta_1^{L+1} & \beta_2^{L+1} & \beta_3^{L+1} & \beta_4^{L+1} \\ X_1 \beta_1^{L+1} & X_2 \beta_2^{L+1} & X_3 \beta_3^{L+1} & X_4 \beta_4^{L+1} \end{vmatrix} = 0, \quad (\text{D12})$$

where $|\beta_1| \leq |\beta_2| \leq |\beta_3| \leq |\beta_4|$. Here, X_j ($j = 1, 2, 3, 4$) are defined as

$$X_j \equiv E_{\text{OBC}} - t_a^+ \beta_j - t_a^- \beta_j^{-1} - V \quad (j = 1, 2, 3, 4). \quad (\text{D13})$$

Simplifying, we obtain the boundary equation (24) from Eq. (D12):

$$X_{1,4} X_{2,3} [(\beta_1 \beta_4)^{L+1} + (\beta_2 \beta_3)^{L+1}] - X_{1,3} X_{2,4} [(\beta_1 \beta_3)^{L+1} + (\beta_2 \beta_4)^{L+1}] + X_{1,2} X_{3,4} [(\beta_1 \beta_2)^{L+1} + (\beta_3 \beta_4)^{L+1}] = 0, \quad (\text{D14})$$

where $X_{i,j}$ ($i, j = 1, 2, 3, 4$) are defined as

$$X_{i,j} \equiv X_i - X_j = t_a^+(\beta_j - \beta_i) + t_a^-(\beta_j^{-1} - \beta_i^{-1}) \quad (i, j = 1, 2, 3, 4). \quad (\text{D15})$$

APPENDIX E: DERIVATION OF EQ. (26)

We start from the characteristic equation of our coupled Hatano-Nelson model with offset:

$$\begin{aligned} t_a^+ t_b^+ \beta^2 + [-(t_a^+ + t_b^+)E_{\text{OBC}} - (t_a^+ - t_b^+)V]\beta + (t_a^+ t_b^- + t_a^- t_b^+ + E_{\text{OBC}}^2 - t_0^2 - V^2) \\ + [-(t_a^- + t_b^-)E_{\text{OBC}} - (t_a^- - t_b^-)V]\beta^{-1} + t_a^- t_b^- \beta^{-2} = 0. \end{aligned} \quad (\text{E1})$$

We consider a perturbative solution up to the second order in t_0 by first expanding in terms of the β s:

$$\begin{cases} \beta_1 \simeq x_-^{(a)} + y_-^{(a)} t_0^2, \\ \beta_2 \simeq x_+^{(a)} + y_+^{(a)} t_0^2, \\ \beta_3 \simeq x_-^{(b)} + y_-^{(b)} t_0^2, \\ \beta_4 \simeq x_+^{(b)} + y_+^{(b)} t_0^2, \end{cases} \quad (\text{E2})$$

where $t_a^+ > t_a^-$, $t_b^+ < t_b^-$, $t_a^+ > t_b^+$, $V > 0$, $|\beta_1| \leq |\beta_2| \leq |\beta_3| \leq |\beta_4|$,

$$\begin{cases} x_{\pm}^{(a)} = \frac{1}{2t_a^+} (E_{\text{OBC}} - V \pm \Delta_a), \\ x_{\pm}^{(b)} = \frac{1}{2t_b^+} (E_{\text{OBC}} + V \pm \Delta_b), \\ y_{\pm}^{(a)} = \frac{-[E_{\text{OBC}}^2 - 2t_a^+ t_a^- + V(V \mp \Delta_a) - (2V \mp \Delta_a)E_{\text{OBC}}]}{g_{\pm}^{(a)}}, \\ y_{\pm}^{(b)} = \frac{[E_{\text{OBC}}^2 - 2t_b^+ t_b^- + V(V \pm \Delta_b) + (2V \pm \Delta_b)E_{\text{OBC}}]}{g_{\pm}^{(b)}}, \end{cases} \quad (\text{E3})$$

and

$$\Delta_a = \sqrt{(E_{\text{OBC}} - V)^2 - 4t_a^+ t_a^-}, \quad (\text{E4})$$

$$\Delta_b = \sqrt{(E_{\text{OBC}} + V)^2 - 4t_b^+ t_b^-}, \quad (\text{E5})$$

$$\begin{aligned} g_{\pm}^{(a)} = E_{\text{OBC}}^3(t_a^+ - t_b^+) - 4t_a^+ t_a^- (t_a^+ + t_b^+)V + (t_a^+ + t_b^+)V^3 \mp 2t_a^+ (t_a^+ t_b^- - t_a^- t_b^+) \Delta_a \\ \mp (t_a^+ + t_b^+) \Delta_a V^2 + E_{\text{OBC}}^2[(3t_b^+ - t_a^+)V \pm (t_a^+ - t_b^+) \Delta_a] \\ + E_{\text{OBC}}[-4t_a^+ t_a^- (t_a^+ - t_b^+) - (t_a^+ + 3t_b^+)V^2 \pm 2t_b^+ \Delta_a V], \end{aligned} \quad (\text{E6})$$

$$\begin{aligned} g_{\pm}^{(b)} = E_{\text{OBC}}^3(t_a^+ - t_b^+) - 4t_b^+ t_b^- (t_a^+ + t_b^+)V + (t_a^+ + t_b^+)V^3 \mp 2t_b^+ (t_a^+ t_b^- - t_a^- t_b^+) \Delta_b \\ \pm (t_a^+ + t_b^+) \Delta_b V^2 + E_{\text{OBC}}^2[(3t_a^+ - t_b^+)V \pm (t_a^+ - t_b^+) \Delta_b] \\ + E_{\text{OBC}}[-4t_b^+ t_b^- (t_a^+ - t_b^+) + (t_b^+ + 3t_a^+)V^2 \pm 2t_a^+ \Delta_b V]. \end{aligned} \quad (\text{E7})$$

With Eqs. (E2) and (D13), we can get

$$\begin{cases} X_{1,2} = \frac{(t_a^+ t_b^- - t_a^- t_b^+) \Delta_a t_0^2}{E_{\text{OBC}}^2(t_a^- - t_b^-)(t_a^+ - t_b^+) + (t_a^+ t_b^- - t_a^- t_b^+)^2 + 2E_{\text{OBC}}V(t_a^+ t_a^- - t_b^+ t_b^-) + (t_a^- + t_b^-)(t_a^+ + t_b^+)V^2} + O(t_0^4), \\ X_{3,4} = \left(\frac{t_a^+}{t_b^+} - \frac{t_a^-}{t_b^-} \right) \Delta_b + O(t_0^2), \\ X_{1,3} = \frac{1}{2} \left[\frac{t_a^+}{t_b^+} (E_{\text{OBC}} + V - \Delta_b) - (E_{\text{OBC}} - V - \Delta_a) \right] + \left[\frac{2t_b^+ t_a^-}{E_{\text{OBC}} + V - \Delta_b} - \frac{2t_a^+ t_a^-}{E_{\text{OBC}} - V - \Delta_a} \right] + O(t_0^2), \\ X_{2,4} = \frac{1}{2} \left[\frac{t_a^+}{t_b^+} (E_{\text{OBC}} + V + \Delta_b) - (E_{\text{OBC}} - V + \Delta_a) \right] + \left[\frac{2t_b^+ t_a^-}{E_{\text{OBC}} + V + \Delta_b} - \frac{2t_a^+ t_a^-}{E_{\text{OBC}} - V + \Delta_a} \right] + O(t_0^2). \end{cases} \quad (\text{E8})$$

We can obtain Eq. (26) by substituting Eq. (E8) into $X_{1,2} X_{3,4} / (X_{1,3} X_{2,4})$ and expanding up to the second order in t_0 .

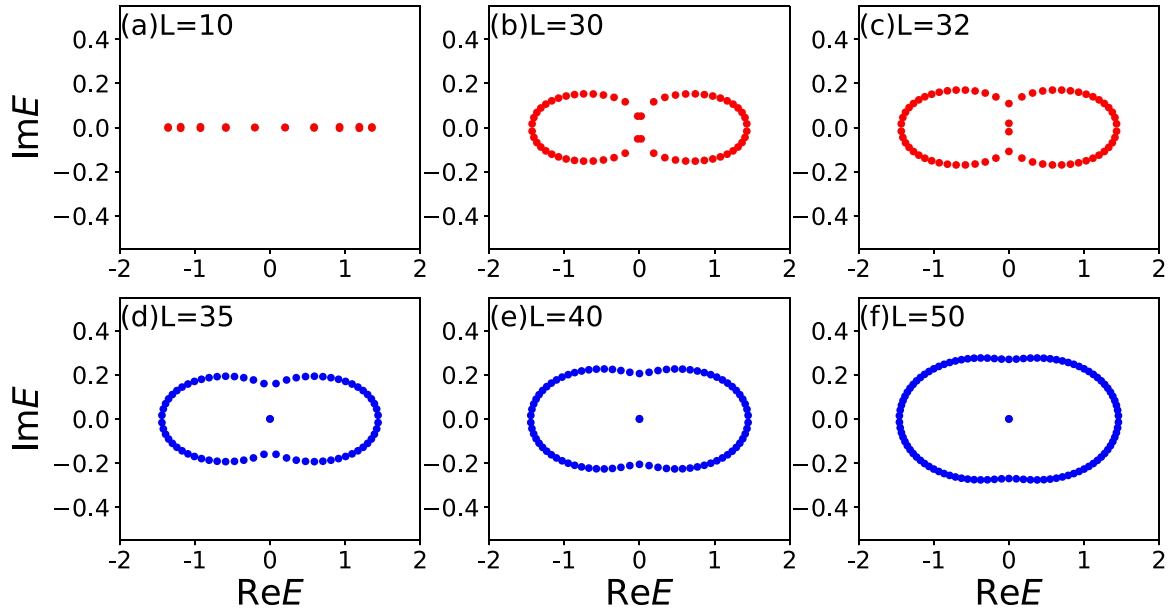


FIG. 13. OBC energy spectra of the topologically coupled chain model Hamiltonian (33) with $V = 0$ at different system sizes (a) $L = 10$, (b) $L = 30$, (c) $L = 32$, (d) $L = 35$, (e) $L = 40$, (f) $L = 50$. Notably, topological zero modes appear at $E = 0$ in the point gap only at sufficiently large system sizes of $L = 35, 40, 50$. The other parameters are $\delta_{ab} = 0.5 \times 10^{-3}$, $t_1 = 0.75$, and $\delta_a = -\delta_b = 0.25$.

APPENDIX F: OBC SPECTRA FOR TOPOLOGICALLY COUPLED CHAIN MODEL

In this Appendix, in order to understand why the topological zero modes appear at $E = 0$ in the point gap only at sufficiently large system sizes, we show the OBC energy spectra of the topologically coupled chain model (33) with $V = 0$ for various system sizes.

It is indicated from Fig. 13 that, when we tune the system size L (regarding L as a parameter), the OBC spectrum changes. At a critical L , the OBC spectrum's gap closes and, after that, topological zero modes appear.

APPENDIX G: DERIVATION OF EQ. (35)

In this Appendix, we describe the derivation of Eq. (35), which expresses the OBC constraint of our coupled topological model. Under OBCs, we can write the real-space Schrödinger equation $\mathcal{H}_t|\psi\rangle = E_{\text{OBC}}|\psi\rangle$ [where \mathcal{H}_t is the Hamiltonian matrix of H_t in the basis $(C_1, C_2, \dots, C_L)^T$], where $|\psi\rangle = (\psi_{1,A}, \psi_{1,B}, \psi_{2,A}, \psi_{2,B}, \dots, \psi_{n,A}, \psi_{n,B}, \dots)^T$, as

$$\begin{cases} t_a^- \psi_{n-1,A} + \delta_{ab} \psi_{n-1,B} + V \psi_{n,A} + t_a^+ \psi_{n+1,A} + \delta_{ab} \psi_{n+1,B} = E_{\text{OBC}} \psi_{n,A}, \\ t_b^- \psi_{n-1,B} - \delta_{ab} \psi_{n-1,A} - V \psi_{n,B} + t_b^+ \psi_{n+1,B} - \delta_{ab} \psi_{n+1,A} = E_{\text{OBC}} \psi_{n,B}. \end{cases} \quad (\text{G1})$$

According to the theory of linear difference equations, we can take as an ansatz for the eigenstates the linear combination

$$\begin{pmatrix} \psi_{n,A} \\ \psi_{n,B} \end{pmatrix} = \sum_{j=1}^4 \beta_j^n \begin{pmatrix} \phi_A^{(j)} \\ \phi_B^{(j)} \end{pmatrix}. \quad (\text{G2})$$

Hence, Eq. (G1) can be rewritten as

$$\begin{pmatrix} t_a^+ \beta + t_a^- \beta^{-1} + V & \delta_{ab}(\beta + \beta^{-1}) \\ -\delta_{ab}(\beta + \beta^{-1}) & t_b^+ \beta + t_b^- \beta^{-1} - V \end{pmatrix} \begin{pmatrix} \phi_A \\ \phi_B \end{pmatrix} = E_{\text{OBC}} \begin{pmatrix} \phi_A \\ \phi_B \end{pmatrix}. \quad (\text{G3})$$

From the real-space eigenequation in Eq. (G1) and the open boundary conditions $\psi_{0,\alpha} = \psi_{L+1,\alpha} = 0$ ($\alpha = A, B$), we can get the equations for the eigenstates in real space as

$$\begin{cases} \delta_{ab} \psi_{2,B} + t_a^+ \psi_{2,A} + V \psi_{1,A} = E_{\text{OBC}} \psi_{1,A}, \\ -\delta_{ab} \psi_{2,A} + t_b^+ \psi_{2,B} - V \psi_{1,B} = E_{\text{OBC}} \psi_{1,B}, \\ t_a^- \psi_{L-1,A} + \delta_{ab} \psi_{L-1,B} + V \psi_{L,A} = E_{\text{OBC}} \psi_{L,A}, \\ t_b^- \psi_{L-1,B} - \delta_{ab} \psi_{L-1,A} - V \psi_{L,B} = E_{\text{OBC}} \psi_{L,B}. \end{cases} \quad (\text{G4})$$

Now, Eq. (G4) can be rewritten into coupled equations for the coefficients $\phi_\alpha^{(j)}$ ($\alpha = A, B; j = 1, 2, 3, 4$) by substituting the general solution $(\psi_{n,A}, \psi_{n,B})^T = \sum_{j=1}^4 \beta_j^n (\phi_A^{(j)}, \phi_B^{(j)})^T$ as

$$\left\{ \begin{array}{l} \delta_{ab} \sum_{j=1}^4 \beta_j^2 \phi_B^{(j)} + t_a^+ \sum_{j=1}^4 \beta_j^2 \phi_A^{(j)} + V \sum_{j=1}^4 \beta_j \phi_A^{(j)} = E_{\text{OBC}} \sum_{j=1}^4 \beta_j \phi_A^{(j)}, \\ -\delta_{ab} \sum_{j=1}^4 \beta_j^2 \phi_A^{(j)} + t_b^+ \sum_{j=1}^4 \beta_j^2 \phi_B^{(j)} - V \sum_{j=1}^4 \beta_j \phi_B^{(j)} = E_{\text{OBC}} \sum_{j=1}^4 \beta_j \phi_B^{(j)}, \\ t_a^- \sum_{j=1}^4 \beta_j^{L-1} \phi_A^{(j)} + \delta_{ab} \sum_{j=1}^4 \beta_j^{L-1} \phi_B^{(j)} + V \sum_{j=1}^4 \beta_j^L \phi_A^{(j)} = E_{\text{OBC}} \sum_{j=1}^4 \beta_j^L \phi_A^{(j)}, \\ t_b^- \sum_{j=1}^4 \beta_j^{L-1} \phi_B^{(j)} - \delta_{ab} \sum_{j=1}^4 \beta_j^{L-1} \phi_A^{(j)} - V \sum_{j=1}^4 \beta_j^L \phi_B^{(j)} = E_{\text{OBC}} \sum_{j=1}^4 \beta_j^L \phi_B^{(j)}. \end{array} \right. \quad (\text{G5})$$

Furthermore, by using the bulk eigenequation in Eq. (G3),

$$\left\{ \begin{array}{l} (t_a^+ \beta + t_a^- \beta^{-1} + V - E_{\text{OBC}}) \phi_A + \delta_{ab} (\beta + \beta^{-1}) \phi_B = 0, \quad \frac{\phi_B}{\phi_A} = -\frac{(t_a^+ \beta + t_a^- \beta^{-1} + V - E_{\text{OBC}})}{\delta_{ab} (\beta + \beta^{-1})}, \\ -\delta_{ab} (\beta + \beta^{-1}) \phi_A + (t_b^+ \beta + t_b^- \beta^{-1} - V - E_{\text{OBC}}) \phi_B = 0, \quad \frac{\phi_B}{\phi_A} = \frac{\delta_{ab} (\beta + \beta^{-1})}{(t_b^+ \beta + t_b^- \beta^{-1} - V - E_{\text{OBC}})}, \end{array} \right. \quad (\text{G6})$$

i.e.,

$$\frac{\phi_B^{(j)}}{\phi_A^{(j)}} = \frac{(E_{\text{OBC}} - t_a^+ \beta_j - t_a^- \beta_j^{-1} - V)}{\delta_{ab} (\beta + \beta^{-1})} = \frac{-\delta_{ab} (\beta + \beta^{-1})}{(E_{\text{OBC}} - t_b^+ \beta_j - t_b^- \beta_j^{-1} + V)} = f_j, \quad (\text{G7})$$

$$-\delta_{ab}^2 (\beta + \beta^{-1})^2 = (E_{\text{OBC}} - t_a^+ \beta_j - t_a^- \beta_j^{-1} - V)(E_{\text{OBC}} - t_b^+ \beta_j - t_b^- \beta_j^{-1} + V), \quad (\text{G8})$$

$$\phi_B^{(j)} = f_j \phi_A^{(j)}. \quad (\text{G9})$$

The general solution is written as a linear combination

$$\begin{pmatrix} \psi_{n,A} \\ \psi_{n,B} \end{pmatrix} = \beta_1^n \begin{pmatrix} \phi_A^{(1)} \\ \phi_B^{(1)} \end{pmatrix} + \beta_2^n \begin{pmatrix} \phi_A^{(2)} \\ \phi_B^{(2)} \end{pmatrix} + \beta_3^n \begin{pmatrix} \phi_A^{(3)} \\ \phi_B^{(3)} \end{pmatrix} + \beta_4^n \begin{pmatrix} \phi_A^{(4)} \\ \phi_B^{(4)} \end{pmatrix} \quad (\text{G10})$$

which should satisfy the open boundary conditions (G5):

$$\left\{ \begin{array}{l} \delta_{ab} \sum_{j=1}^4 \beta_j^2 f_j \phi_A^{(j)} + t_a^+ \sum_{j=1}^4 \beta_j^2 \phi_A^{(j)} + V \sum_{j=1}^4 \beta_j \phi_A^{(j)} = E_{\text{OBC}} \sum_{j=1}^4 \beta_j \phi_A^{(j)}, \\ -\delta_{ab} \sum_{j=1}^4 \beta_j^2 \phi_A^{(j)} + t_b^+ \sum_{j=1}^4 \beta_j^2 f_j \phi_A^{(j)} - V \sum_{j=1}^4 \beta_j f_j \phi_A^{(j)} = E_{\text{OBC}} \sum_{j=1}^4 \beta_j f_j \phi_A^{(j)}, \\ t_a^- \sum_{j=1}^4 \beta_j^{L-1} \phi_A^{(j)} + \delta_{ab} \sum_{j=1}^4 \beta_j^{L-1} f_j \phi_A^{(j)} + V \sum_{j=1}^4 \beta_j^L \phi_A^{(j)} = E_{\text{OBC}} \sum_{j=1}^4 \beta_j^L \phi_A^{(j)}, \\ t_b^- \sum_{j=1}^4 \beta_j^{L-1} f_j \phi_A^{(j)} - \delta_{ab} \sum_{j=1}^4 \beta_j^{L-1} \phi_A^{(j)} - V \sum_{j=1}^4 \beta_j^L f_j \phi_A^{(j)} = E_{\text{OBC}} \sum_{j=1}^4 \beta_j^L f_j \phi_A^{(j)}, \end{array} \right. \quad (\text{G11})$$

$$\left\{ \begin{aligned} \sum_{j=1}^4 \frac{(E_{\text{OBC}} - t_a^+ \beta_j - t_a^- \beta_j^{-1} - V)}{\beta_j + \beta_j^{-1}} \beta_j^2 \phi_A^{(j)} &= \sum_{j=1}^4 (E_{\text{OBC}} - t_a^+ \beta_j - V) \beta_j \phi_A^{(j)}, \\ -\delta_{ab} \sum_{j=1}^4 \beta_j^2 \phi_A^{(j)} + \sum_{j=1}^4 (t_b^+ \beta_j - V - E_{\text{OBC}}) \beta_j f_j \phi_A^{(j)} &= 0, \\ \sum_{j=1}^4 \frac{(E_{\text{OBC}} - t_a^+ \beta_j - t_a^- \beta_j^{-1} - V)}{\beta_j + \beta_j^{-1}} \beta_j^{L-1} \phi_A^{(j)} &= \sum_{j=1}^4 (E_{\text{OBC}} - t_a^- \beta_j^{-1} - V) \beta_j^L \phi_A^{(j)}, \\ \sum_{j=1}^4 (t_b^- \beta_j^{-1} - V - E_{\text{OBC}}) \beta_j^L f_j \phi_A^{(j)} - \delta_{ab} \sum_{j=1}^4 \beta_j^{L-1} \phi_A^{(j)} &= 0, \end{aligned} \right. \tag{G12}$$

$$\left\{ \begin{aligned} \sum_{j=1}^4 [(E_{\text{OBC}} - t_a^+ \beta_j - t_a^- \beta_j^{-1} - V) \beta_j - (E_{\text{OBC}} - t_a^+ \beta_j - V)(\beta_j + \beta_j^{-1})] \beta_j \phi_A^{(j)} &= 0, \\ \sum_{j=1}^4 \beta_j^2 \phi_A^{(j)} + \sum_{j=1}^4 \frac{(\beta_j + \beta_j^{-1})(t_b^+ \beta_j - V - E_{\text{OBC}})}{(E_{\text{OBC}} - t_b^+ \beta_j - t_b^- \beta_j^{-1} + V)} \beta_j \phi_A^{(j)} &= 0, \\ \sum_{j=1}^4 [(E_{\text{OBC}} - t_a^+ \beta_j - t_a^- \beta_j^{-1} - V) \beta_j^{-1} - (E_{\text{OBC}} - t_a^- \beta_j^{-1} - V)(\beta_j + \beta_j^{-1})] \beta_j^L \phi_A^{(j)} &= 0, \\ \sum_{j=1}^4 \frac{(\beta_j + \beta_j^{-1})(t_b^- \beta_j^{-1} - V - E_{\text{OBC}})}{(E_{\text{OBC}} - t_b^+ \beta_j - t_b^- \beta_j^{-1} + V)} \beta_j^L \phi_A^{(j)} + \sum_{j=1}^4 \beta_j^{L-1} \phi_A^{(j)} &= 0, \end{aligned} \right. \tag{G13}$$

$$\left\{ \begin{aligned} \sum_{j=1}^4 [-t_a^- - (E_{\text{OBC}} - t_a^+ \beta_j - V) \beta_j^{-1}] \beta_j \phi_A^{(j)} &= 0, \\ \sum_{j=1}^4 [(E_{\text{OBC}} - t_b^+ \beta_j - t_b^- \beta_j^{-1} + V) \beta_j - (E_{\text{OBC}} - t_b^+ \beta_j + V)(\beta_j + \beta_j^{-1})] \beta_j \phi_A^{(j)} &= 0, \\ \sum_{j=1}^4 [-t_a^+ - (E_{\text{OBC}} - t_a^- \beta_j^{-1} - V) \beta_j] \beta_j^L \phi_A^{(j)} &= 0, \\ \sum_{j=1}^4 [(E_{\text{OBC}} - t_b^+ \beta_j - t_b^- \beta_j^{-1} + V) \beta_j^{-1} - (E_{\text{OBC}} - t_b^- \beta_j^{-1} + V)(\beta_j + \beta_j^{-1})] \beta_j^L \phi_A^{(j)} &= 0, \end{aligned} \right. \tag{G14}$$

$$\left\{ \begin{aligned} \sum_{j=1}^4 [-t_a^- - (E_{\text{OBC}} - t_a^+ \beta_j - V) \beta_j^{-1}] \beta_j \phi_A^{(j)} &= 0, \\ \sum_{j=1}^4 [-t_b^- - (E_{\text{OBC}} - t_b^+ \beta_j + V) \beta_j^{-1}] \beta_j \phi_A^{(j)} &= 0, \\ \sum_{j=1}^4 [-t_a^+ - (E_{\text{OBC}} - t_a^- \beta_j^{-1} - V) \beta_j] \beta_j^L \phi_A^{(j)} &= 0, \\ \sum_{j=1}^4 [-t_b^+ - (E_{\text{OBC}} - t_b^- \beta_j^{-1} + V) \beta_j] \beta_j^L \phi_A^{(j)} &= 0, \end{aligned} \right. \tag{G15}$$

$$\left\{ \begin{array}{l} \sum_{j=1}^4 [E_{\text{OBC}} - (t_a^+ - t_a^-)\beta_j - V]\phi_A^{(j)} = 0, \\ \sum_{j=1}^4 [E_{\text{OBC}} - (t_b^+ - t_b^-)\beta_j + V]\phi_A^{(j)} = 0, \\ \sum_{j=1}^4 [E_{\text{OBC}} + (t_a^+ - t_a^-)\beta_j^{-1} - V]\beta_j^{L+1}\phi_A^{(j)} = 0, \\ \sum_{j=1}^4 [E_{\text{OBC}} + (t_b^+ - t_b^-)\beta_j^{-1} + V]\beta_j^{L+1}\phi_A^{(j)} = 0. \end{array} \right. \quad (\text{G16})$$

Here, we have obtained the coupled equations in terms of only $\phi_A^{(j)}$ ($j = 1, 2, 3, 4$). For $\phi_A^{(j)}$ ($j = 1, 2, 3, 4$) to have nonzero values, the determinant condition is

$$\begin{vmatrix} X_1^{(a)} & X_2^{(a)} & X_3^{(a)} & X_4^{(a)} \\ Y_1^{(a)} & Y_2^{(a)} & Y_3^{(a)} & Y_4^{(a)} \\ X_1^{(b)}\beta_1^{L+1} & X_2^{(b)}\beta_2^{L+1} & X_3^{(b)}\beta_3^{L+1} & X_4^{(b)}\beta_4^{L+1} \\ Y_1^{(b)}\beta_1^{L+1} & Y_2^{(b)}\beta_2^{L+1} & Y_3^{(b)}\beta_3^{L+1} & Y_4^{(b)}\beta_4^{L+1} \end{vmatrix} = 0 \quad (\text{G17})$$

with $|\beta_1| \leq |\beta_2| \leq |\beta_3| \leq |\beta_4|$. Here, X_j and Y_j ($j = 1, \dots, 4$) are defined as

$$X_j^{(a)} = E_{\text{OBC}} - (t_a^+ - t_a^-)\beta_j - V = E_{\text{OBC}} - 2\delta_a\beta_j - V \quad (j = 1, \dots, 4), \quad (\text{G18})$$

$$Y_j^{(a)} = E_{\text{OBC}} - (t_b^+ - t_b^-)\beta_j + V = E_{\text{OBC}} - 2\delta_b\beta_j + V \quad (j = 1, \dots, 4), \quad (\text{G19})$$

$$X_j^{(b)} = E_{\text{OBC}} + (t_a^+ - t_a^-)\beta_j^{-1} - V = E_{\text{OBC}} + 2\delta_a\beta_j^{-1} - V \quad (j = 1, \dots, 4), \quad (\text{G20})$$

$$Y_j^{(b)} = E_{\text{OBC}} + (t_b^+ - t_b^-)\beta_j^{-1} + V = E_{\text{OBC}} + 2\delta_b\beta_j^{-1} + V \quad (j = 1, \dots, 4). \quad (\text{G21})$$

Finally, we can obtain the boundary equation (35) from Eq. (G17) as

$$\begin{aligned} & [Z_{1,4}^{(b)}Z_{2,3}^{(a)}(\beta_1\beta_4)^{L+1} + Z_{1,4}^{(a)}Z_{2,3}^{(b)}(\beta_2\beta_3)^{L+1}] \\ & - [Z_{1,3}^{(b)}Z_{2,4}^{(a)}(\beta_1\beta_3)^{L+1} + Z_{1,3}^{(a)}Z_{2,4}^{(b)}(\beta_2\beta_4)^{L+1}] \\ & + [Z_{1,2}^{(b)}Z_{3,4}^{(a)}(\beta_1\beta_2)^{L+1} + Z_{1,2}^{(a)}Z_{3,4}^{(b)}(\beta_3\beta_4)^{L+1}] = 0, \end{aligned} \quad (\text{G22})$$

where β_j ($j = 1, 2, 3, 4$) satisfy $|\beta_1| \leq |\beta_2| \leq |\beta_3| \leq |\beta_4|$, and $Z_{i,j}^{(c)}$ ($i, j = 1, 2, 3, 4; c = a, b$) are defined as

$$Z_{i,j}^{(c)} = X_i^{(c)}Y_j^{(c)} - X_j^{(c)}Y_i^{(c)} \quad (\text{G23})$$

$$= \begin{cases} [(t_b^+ - t_b^-)(E_{\text{OBC}} - V) - (t_a^+ - t_a^-)(E_{\text{OBC}} + V)](\beta_i - \beta_j), & c = a \\ [(t_b^+ - t_b^-)(E_{\text{OBC}} - V) - (t_a^+ - t_a^-)(E_{\text{OBC}} + V)](\beta_j^{-1} - \beta_i^{-1}), & c = b \end{cases} \quad (\text{G24})$$

where $i, j = 1, 2, 3, 4; c = a, b$.

-
- [1] Q. Zhong, J. Ren, M. Khajavikhan, D. N. Christodoulides, Ş. K. Özdemir, and R. El-Ganainy, Sensing with Exceptional Surfaces in Order to Combine Sensitivity with Robustness, *Phys. Rev. Lett.* **122**, 153902 (2019).
- [2] P. Djourwe, Y. Pennec, and B. Djafari-Rouhani, Exceptional Point Enhances Sensitivity of Optomechanical Mass Sensors, *Phys. Rev. Appl.* **12**, 024002 (2019).
- [3] Z. Guo, T. Zhang, J. Song, H. Jiang, and H. Chen, Sensitivity of topological edge states in a non-hermitian dimer chain, *Photonics Res.* **9**, 574 (2021).
- [4] C. Chen, Y. Xie, and S.-W. Huang, Nanophotonic optical gyroscope with sensitivity enhancement around mirrored exceptional points, *Opt. Commun.* **483**, 126674 (2021).
- [5] C. Chen, L. Jin, and R.-B. Liu, Sensitivity of parameter estimation near the exceptional point of a non-hermitian system, *New J. Phys.* **21**, 083002 (2019).
- [6] A. Nikzamid, K. Rouhi, A. Figotin, and F. Capolino, How to achieve exceptional points in coupled resonators using a gyration or pt-symmetry, and in a time-modulated single resonator: High sensitivity to perturbations, *EPJ Appl. Metamater.* **9**, 14 (2022).
- [7] C. H. Lee, Exceptional Bound States and Negative Entanglement Entropy, *Phys. Rev. Lett.* **128**, 010402 (2022).

- [8] P.-Y. Chang, J.-S. You, X. Wen, and S. Ryu, Entanglement spectrum and entropy in topological non-hermitian systems and nonunitary conformal field theory, *Phys. Rev. Res.* **2**, 033069 (2020).
- [9] B. Dóra, D. Sticlet, and C. P. Moca, Correlations at PT-Symmetric Quantum Critical Point, *Phys. Rev. Lett.* **128**, 146804 (2022).
- [10] Y.-C. Wang, H. H. Jen, and J.-S. You, Scaling laws for non-hermitian skin effect with long-range couplings, [arXiv:2211.16565](https://arxiv.org/abs/2211.16565).
- [11] H. Zhou, J. Y. Lee, S. Liu, and B. Zhen, Exceptional surfaces in pt-symmetric non-hermitian photonic systems, *Optica* **6**, 190 (2019).
- [12] X. Zhang, G. Li, Y. Liu, T. Tai, R. Thomale, and C. H. Lee, Tidal surface states as fingerprints of non-Hermitian nodal knot metals, *Commun. Phys.* **4**, 47 (2021).
- [13] J. Wiersig, Robustness of exceptional-point-based sensors against parametric noise: The role of hamiltonian and liouvillian degeneracies, *Phys. Rev. A* **101**, 053846 (2020).
- [14] J. Wiersig, Prospects and fundamental limits in exceptional point-based sensing, *Nat. Commun.* **11**, 2454 (2020).
- [15] J. Wiersig, Review of exceptional point-based sensors, *Photonics Res.* **8**, 1457 (2020).
- [16] G.-L. Zhu, A. Targholizadeh, X.-Y. Lu, C. Yuce, and H. Ramezani, Exceptional point generated robust asymmetric high-order harmonics, [arXiv:2201.07663](https://arxiv.org/abs/2201.07663).
- [17] L. Xiao, T. Deng, K. Wang, Z. Wang, W. Yi, and P. Xue, Observation of Non-Bloch Parity-Time Symmetry and Exceptional Points, *Phys. Rev. Lett.* **126**, 230402 (2021).
- [18] Y. Ashida, Z. Gong, and M. Ueda, Non-hermitian physics, *Adv. Phys.* **69**, 249 (2020).
- [19] R. El-Ganainy, K. G. Makris, M. Khajavikhan, Z. H. Muslimani, S. Rotter, and D. N. Christodoulides, Non-hermitian physics and PT symmetry, *Nat. Phys.* **14**, 11 (2018).
- [20] K. Kawabata, K. Shiozaki, M. Ueda, and M. Sato, Symmetry and Topology in Non-Hermitian Physics, *Phys. Rev. X* **9**, 041015 (2019).
- [21] E. J. Bergholtz, J. C. Budich, and F. K. Kunst, Exceptional topology of non-hermitian systems, *Rev. Mod. Phys.* **93**, 015005 (2021).
- [22] M. Nakagawa and N. Kawakami, Nonequilibrium topological phase transitions in two-dimensional optical lattices, *Phys. Rev. A* **89**, 013627 (2014).
- [23] L. Xiao, T. Deng, K. Wang, G. Zhu, Z. Wang, W. Yi, and P. Xue, Non-hermitian bulk-boundary correspondence in quantum dynamics, *Nat. Phys.* **16**, 761 (2020).
- [24] F. Song, S. Yao, and Z. Wang, Non-Hermitian Skin Effect and Chiral Damping in Open Quantum Systems, *Phys. Rev. Lett.* **123**, 170401 (2019).
- [25] L. Zhang, W. Jia, and X.-J. Liu, Universal topological quench dynamics: Altland-zirnbauer tenfold classes, *Sci. Bull.*, **67**, 1236 (2022).
- [26] D. Yu, B. Peng, X. Chen, X.-J. Liu, and L. Yuan, Topological holographic quench dynamics in a synthetic frequency dimension, *Light Sci. Appl.* **10**, 209 (2021).
- [27] W. Jia, L. Zhang, L. Zhang, and X.-J. Liu, Dynamically characterizing topological phases by high-order topological charges, *Phys. Rev. A* **103**, 052213 (2021).
- [28] L. Zhang, L. Zhang, and X.-J. Liu, Quench-induced dynamical topology under dynamical noise, *Phys. Rev. Res.* **3**, 013229 (2021).
- [29] X.-L. Yu, W. Ji, L. Zhang, Y. Wang, J. Wu, and X.-J. Liu, Quantum dynamical characterization and simulation of topological phases with high-order band inversion surfaces, *PRX Quantum* **2**, 020320 (2021).
- [30] L. Zhang, L. Zhang, and X.-J. Liu, Unified Theory to Characterize Floquet Topological Phases by Quench Dynamics, *Phys. Rev. Lett.* **125**, 183001 (2020).
- [31] C.-R. Yi, L. Zhang, L. Zhang, R.-H. Jiao, X.-C. Cheng, Z.-Y. Wang, X.-T. Xu, W. Sun, X.-J. Liu, S. Chen, and J.-W. Pan, Observing Topological Charges and Dynamical Bulk-Surface Correspondence with Ultracold Atoms, *Phys. Rev. Lett.* **123**, 190603 (2019).
- [32] Y. Wang, W. Ji, Z. Chai, Y. Guo, M. Wang, X. Ye, P. Yu, L. Zhang, X. Qin, P. Wang *et al.*, Experimental observation of dynamical bulk-surface correspondence in momentum space for topological phases, *Phys. Rev. A* **100**, 052328 (2019).
- [33] L. Zhang, L. Zhang, Y. Hu, S. Niu, and X.-J. Liu, Nonequilibrium characterization of equilibrium correlated quantum phases, *Phys. Rev. B* **103**, 224308 (2021).
- [34] W. Sun, C.-R. Yi, B.-Z. Wang, W.-W. Zhang, B. C. Sanders, X.-T. Xu, Z.-Y. Wang, J. Schmiedmayer, Y. Deng, X.-J. Liu, S. Chen, and J.-W. Pan, Uncover Topology by Quantum Quench Dynamics, *Phys. Rev. Lett.* **121**, 250403 (2018).
- [35] L. Zhang, L. Zhang, S. Niu, and X.-J. Liu, Dynamical classification of topological quantum phases, *Sci. Bull.* **63**, 1385 (2018).
- [36] J. Li, A. K. Harter, J. Liu, L. de Melo, Y. N. Joglekar, and L. Luo, Observation of parity-time symmetry breaking transitions in a dissipative floquet system of ultracold atoms, *Nat. Commun.* **10**, 1 (2019).
- [37] S. Lapp, J. Ang'ong'a, F. A. An, and B. Gadway, Engineering tunable local loss in a synthetic lattice of momentum states, *New J. Phys.* **21**, 045006 (2019).
- [38] Z. Ren, D. Liu, E. Zhao, C. He, K. K. Pak, J. Li, and G.-B. Jo, Chiral control of quantum states in non-hermitian spin-orbit-coupled fermions, *Nat. Phys.* **18**, 385 (2022).
- [39] Q. Liang, D. Xie, Z. Dong, H. Li, H. Li, B. Gadway, W. Yi, and B. Yan, Dynamic Signatures of Non-Hermitian Skin Effect and Topology in Ultracold Atoms, *Phys. Rev. Lett.* **129**, 070401 (2022).
- [40] W. Gou, T. Chen, D. Xie, T. Xiao, T.-S. Deng, B. Gadway, W. Yi, and B. Yan, Tunable Nonreciprocal Quantum Transport through a Dissipative Aharonov-Bohm Ring in Ultracold Atoms, *Phys. Rev. Lett.* **124**, 070402 (2020).
- [41] T. Helbig, T. Hofmann, S. Imhof, M. Abdelghany, T. Kiessling, L. W. Molenkamp, C. H. Lee, A. Szameit, M. Greiter, and R. Thomale, Generalized bulk-boundary correspondence in non-hermitian topoelectrical circuits, *Nat. Phys.* **16**, 747 (2020).
- [42] T. Hofmann, T. Helbig, C. H. Lee, M. Greiter, and R. Thomale, Chiral Voltage Propagation and Calibration in a Topoelectrical Chern Circuit, *Phys. Rev. Lett.* **122**, 247702 (2019).
- [43] S. Liu, S. Ma, C. Yang, L. Zhang, W. Gao, Y. J. Xiang, T. J. Cui, and S. Zhang, Gain- and Loss-Induced Topological Insulating Phase in a Non-Hermitian Electrical Circuit, *Phys. Rev. Appl.* **13**, 014047 (2020).

- [44] S. Liu, R. Shao, S. Ma, L. Zhang, O. You, H. Wu, Y. J. Xiang, T. J. Cui, and S. Zhang, Non-Hermitian skin effect in a non-Hermitian electrical circuit, *Research* **2021**, 5608038 (2021).
- [45] D. Zou, T. Chen, W. He, J. Bao, C. H. Lee, H. Sun, and X. Zhang, Observation of hybrid higher-order skin-topological effect in non-Hermitian topoelectrical circuits, *Nat. Commun.* **12**, 7201 (2021).
- [46] A. Stegmaier, S. Imhof, T. Helbig, T. Hofmann, C. H. Lee, M. Kremer, A. Fritzsche, T. Feichtner, S. Klembt, S. Höfling, I. Boettcher, I. C. Fulga, L. Ma, O. G. Schmidt, M. Greiter, T. Kiessling, A. Szameit, and R. Thomale, Topological Defect Engineering and \mathcal{PT} Symmetry in Non-Hermitian Electrical Circuits, *Phys. Rev. Lett.* **126**, 215302 (2021).
- [47] H. Hohmann, T. Hofmann, T. Helbig, S. Imhof, H. Brand, L. K. Upreti, A. Stegmaier, A. Fritzsche, T. Müller, U. Schwingenschlögl *et al.*, Observation of cnoidal wave localization in non-linear topoelectric circuits, [arXiv:2206.09931](https://arxiv.org/abs/2206.09931).
- [48] B. Lv, R. Chen, R. Li, C. Guan, B. Zhou, G. Dong, C. Zhao, Y. Li, Y. Wang, H. Tao *et al.*, Realization of quasicrystalline quadrupole topological insulators in electrical circuits, *Commun. Phys.* **4**, 108 (2021).
- [49] X. Zhang, B. Zhang, H. Sahin, Z. B. Siu, S. M. Rafi-Ul-Islam, J. F. Kong, M. Jalil, R. Thomale, and C. H. Lee, Anomalous fractal scaling in two-dimensional electric networks, [arXiv:2204.05329](https://arxiv.org/abs/2204.05329).
- [50] P. M. Lengenbacher, A. Stegmaier, L. K. Upreti, T. Hofmann, T. Helbig, A. Vollhardt, M. Greiter, C. H. Lee, S. Imhof, H. Brand *et al.*, Simulating hyperbolic space on a circuit board, *Nat. Commun.* **13**, 4373 (2022).
- [51] C. Shang, S. Liu, R. Shao, P. Han, X. Zang, X. Zhang, K. N. Salama, W. Gao, C. H. Lee, R. Thomale, A. Manchon, S. Zhang, T. J. Cui, and U. Schwingenschlögl, Experimental identification of the second-order non-Hermitian skin effect with physics-graph-informed machine learning, *Adv. Sci.* **9**, 2202922 (2022).
- [52] X. Zhang, B. Zhang, W. Zhao, and C. H. Lee, Observation of non-local impedance response in a passive electrical circuit, [arXiv:2211.09152](https://arxiv.org/abs/2211.09152).
- [53] M. Wu, Q. Zhao, L. Kang, M. Weng, Z. Chi, R. Peng, J. Liu, D. H. Werner, Y. Meng, and J. Zhou, Evidencing non-Bloch dynamics in temporal topoelectrical circuits, *Phys. Rev. B* **107**, 064307 (2023).
- [54] F. Roccati, S. Lorenzo, G. Calajò, G. M. Palma, A. Carollo, and F. Ciccarello, Exotic interactions mediated by a non-hermitian photonic bath, *Optica* **9**, 565 (2022).
- [55] L. Feng, R. El-Ganainy, and L. Ge, Non-hermitian photonics based on parity-time symmetry, *Nat. Photonics* **11**, 752 (2017).
- [56] L. D. Tzuang, K. Fang, P. Nussenzeig, S. Fan, and M. Lipson, Non-reciprocal phase shift induced by an effective magnetic flux for light, *Nat. Photonics* **8**, 701 (2014).
- [57] H. Zhou, C. Peng, Y. Yoon, C. W. Hsu, K. A. Nelson, L. Fu, J. D. Joannopoulos, M. Soljačić, and B. Zhen, Observation of bulk fermi arc and polarization half charge from paired exceptional points, *Science* **359**, 1009 (2018).
- [58] B. Zhen, C. W. Hsu, Y. Igarashi, L. Lu, I. Kaminer, A. Pick, S.-L. Chua, J. D. Joannopoulos, and M. Soljačić, Spawning rings of exceptional points out of dirac cones, *Nature (London)* **525**, 354 (2015).
- [59] J. M. Zeuner, M. C. Rechtsman, Y. Plotnik, Y. Lumer, S. Nolte, M. S. Rudner, M. Segev, and A. Szameit, Observation of a Topological Transition in the Bulk of a Non-Hermitian System, *Phys. Rev. Lett.* **115**, 040402 (2015).
- [60] M.-A. Miri and A. Alù, Exceptional points in optics and photonics, *Science* **363**, eaar7709 (2019).
- [61] L. Feng, M. Ayache, J. Huang, Y.-L. Xu, M.-H. Lu, Y.-F. Chen, Y. Fainman, and A. Scherer, Nonreciprocal light propagation in a silicon photonic circuit, *Science* **333**, 729 (2011).
- [62] Z. Shen, Y.-L. Zhang, Y. Chen, C.-L. Zou, Y.-F. Xiao, X.-B. Zou, F.-W. Sun, G.-C. Guo, and C.-H. Dong, Experimental realization of optomechanically induced non-reciprocity, *Nat. Photonics* **10**, 657 (2016).
- [63] K. Ding, G. Ma, M. Xiao, Z. Q. Zhang, and C. T. Chan, Emergence, Coalescence, and Topological Properties of Multiple Exceptional Points and Their Experimental Realization, *Phys. Rev. X* **6**, 021007 (2016).
- [64] W. Tang, X. Jiang, K. Ding, Y.-X. Xiao, Z.-Q. Zhang, C. T. Chan, and G. Ma, Exceptional nexus with a hybrid topological invariant, *Science* **370**, 1077 (2020).
- [65] K. Ding, G. Ma, Z. Q. Zhang, and C. T. Chan, Experimental Demonstration of an Anisotropic Exceptional Point, *Phys. Rev. Lett.* **121**, 085702 (2018).
- [66] W. Tang, K. Ding, and G. Ma, Direct Measurement of Topological Properties of an Exceptional Parabola, *Phys. Rev. Lett.* **127**, 034301 (2021).
- [67] W. Tang, K. Ding, and G. Ma, Experimental realization of non-abelian permutations in a three-state non-hermitian system, *Natl. Sci. Rev.* **9**, nwac010 (2022).
- [68] S. H. Park, S.-G. Lee, S. Baek, T. Ha, S. Lee, B. Min, S. Zhang, M. Lawrence, and T.-T. Kim, Observation of an exceptional point in a non-hermitian metasurface, *Nanophotonics* **9**, 1031 (2020).
- [69] C. Coulais, D. Sounas, and A. Alu, Static non-reciprocity in mechanical metamaterials, *Nature (London)* **542**, 461 (2017).
- [70] W. Zhu, X. Fang, D. Li, Y. Sun, Y. Li, Y. Jing, and H. Chen, Simultaneous Observation of a Topological Edge State and Exceptional Point in an Open and Non-Hermitian Acoustic System, *Phys. Rev. Lett.* **121**, 124501 (2018).
- [71] A. Ghatak, M. Brandenbourger, J. Van Wezel, and C. Coulais, Observation of non-hermitian topology and its bulk-edge correspondence in an active mechanical metamaterial, *Proc. Natl. Acad. Sci. USA* **117**, 29561 (2020).
- [72] M. Brandenbourger, X. Locsin, E. Lerner, and C. Coulais, Non-reciprocal robotic metamaterials, *Nat. Commun.* **10**, 4608 (2019).
- [73] H. Gao, H. Xue, Z. Gu, T. Liu, J. Zhu, and B. Zhang, Non-Hermitian route to higher-order topology in an acoustic crystal, *Nat. Commun.* **12**, 1888 (2021).
- [74] F. Qin, C. H. Lee, and R. Chen, Light-induced phase crossovers in a quantum spin hall system, *Phys. Rev. B* **106**, 235405 (2022).
- [75] J. Wang, S. Valligatla, S. Li, Y. Yin, L. Schwarz, M. Medina-Sanchez, S. Baunack, C. H. Lee, R. Thomale, V. M. Fomin *et al.*, Experimental observation of berry phases in optical moebius-strip microcavities, *Nat. Photon.* **17**, 120 (2023).
- [76] Z. Gu, H. Gao, P.-C. Cao, T. Liu, X.-F. Zhu, and J. Zhu, Controlling Sound in Non-Hermitian Acoustic Systems, *Phys. Rev. Appl.* **16**, 057001 (2021).

- [77] F. Qin, R. Chen, and H.-Z. Lu, Phase transitions in intrinsic magnetic topological insulator with high-frequency pumping, *J. Phys.: Condens. Matter* **34**, 225001 (2022).
- [78] X. Wen, X. Zhu, A. Fan, W. Y. Tam, J. Zhu, H. W. Wu, F. Lemoult, M. Fink, and J. Li, Unidirectional amplification with acoustic non-hermitian space-time varying metamaterial, *Commun. Phys.* **5**, 18 (2022).
- [79] F. Qin, S. Li, Z. Z. Du, C. M. Wang, W. Zhang, D. Yu, H.-Z. Lu, and X. C. Xie, Theory for the Charge-Density-Wave Mechanism of 3D Quantum Hall Effect, *Phys. Rev. Lett.* **125**, 206601 (2020).
- [80] A. Gupta and R. Thevamaran, Requisites on viscoelasticity for exceptional points in passive elastodynamic metamaterials, [arXiv:2209.04960](https://arxiv.org/abs/2209.04960).
- [81] C.-K. Chiu, H. Yao, and S. Ryu, Classification of topological insulators and superconductors in the presence of reflection symmetry, *Phys. Rev. B* **88**, 075142 (2013).
- [82] C.-K. Chiu, J. C. Y. Teo, A. P. Schnyder, and S. Ryu, Classification of topological quantum matter with symmetries, *Rev. Mod. Phys.* **88**, 035005 (2016).
- [83] A. C. Potter, T. Morimoto, and A. Vishwanath, Classification of Interacting Topological Floquet Phases in One Dimension, *Phys. Rev. X* **6**, 041001 (2016).
- [84] M. Barkeshli, C.-M. Jian, and X.-L. Qi, Classification of topological defects in abelian topological states, *Phys. Rev. B* **88**, 241103(R) (2013).
- [85] M. McGinley and N. R. Cooper, Classification of topological insulators and superconductors out of equilibrium, *Phys. Rev. B* **99**, 075148 (2019).
- [86] D. V. Else and C. Nayak, Classification of topological phases in periodically driven interacting systems, *Phys. Rev. B* **93**, 201103(R) (2016).
- [87] S. Yao and Z. Wang, Edge States and Topological Invariants of Non-Hermitian Systems, *Phys. Rev. Lett.* **121**, 086803 (2018).
- [88] Y. Xiong, Why does bulk boundary correspondence fail in some non-hermitian topological models, *J. Phys. Commun.* **2**, 035043 (2018).
- [89] C. H. Lee and R. Thomale, Anatomy of skin modes and topology in non-hermitian systems, *Phys. Rev. B* **99**, 201103(R) (2019).
- [90] F. K. Kunst, E. Edvardsson, J. C. Budich, and E. J. Bergholtz, Biorthogonal Bulk-Boundary Correspondence in Non-Hermitian Systems, *Phys. Rev. Lett.* **121**, 026808 (2018).
- [91] K. Yokomizo and S. Murakami, Non-Bloch Band Theory of Non-Hermitian Systems, *Phys. Rev. Lett.* **123**, 066404 (2019).
- [92] K.-I. Imura and Y. Takane, Generalized bulk-edge correspondence for non-hermitian topological systems, *Phys. Rev. B* **100**, 165430 (2019).
- [93] L. Jin and Z. Song, Bulk-boundary correspondence in a non-hermitian system in one dimension with chiral inversion symmetry, *Phys. Rev. B* **99**, 081103(R) (2019).
- [94] D. S. Borgnia, A. J. Kruchkov, and R.-J. Slager, Non-Hermitian Boundary Modes and Topology, *Phys. Rev. Lett.* **124**, 056802 (2020).
- [95] L. Li, S. Mu, C. H. Lee, and J. Gong, Quantized classical response from spectral winding topology, *Nat. Commun.* **12**, 5294 (2021).
- [96] C. Lv, R. Zhang, and Q. Zhou, Curving the space by non-hermiticity, *Nat. Commun.* **13**, 2184 (2022).
- [97] R. Yang, J. W. Tan, T. Tai, J. M. Koh, L. Li, S. Longhi, and C. H. Lee, Designing non-hermitian real spectra through electrostatics, *Sci. Bull.*, **67**, 1865 (2022).
- [98] H. Jiang and C. H. Lee, Dimensional transmutation from non-hermiticity, [arXiv:2207.08843](https://arxiv.org/abs/2207.08843).
- [99] T. Tai and C. H. Lee, Zoology of non-hermitian spectra and their graph topology, [arXiv:2202.03462](https://arxiv.org/abs/2202.03462).
- [100] C. H. Lee, Many-body topological and skin states without open boundaries, *Phys. Rev. B* **104**, 195102 (2021).
- [101] C. H. Lee, L. Li, R. Thomale, and J. Gong, Unraveling non-hermitian pumping: Emergent spectral singularities and anomalous responses, *Phys. Rev. B* **102**, 085151 (2020).
- [102] L. Li and C. H. Lee, Non-hermitian pseudo-gaps, *Sci. Bull.* **67**, 685 (2022).
- [103] R. Shen and C. H. Lee, Non-hermitian skin clusters from strong interactions, *Commun. Phys.* **5**, 238 (2022).
- [104] F. Qin, R. Shen, and C. H. Lee, Non-Hermitian squeezed polarons, *Phys. Rev. A* **107**, L010202 (2023).
- [105] C. H. Lee, L. Li, and J. Gong, Hybrid Higher-Order Skin-Topological Modes in Nonreciprocal Systems, *Phys. Rev. Lett.* **123**, 016805 (2019).
- [106] K. Kawabata, N. Okuma, and M. Sato, Non-bloch band theory of non-hermitian hamiltonians in the symplectic class, *Phys. Rev. B* **101**, 195147 (2020).
- [107] K. Yokomizo and S. Murakami, Non-bloch band theory and bulk-edge correspondence in non-hermitian systems, *Prog. Theor. Exp. Phys.* **2020**, 12A102 (2020).
- [108] Y. Yi and Z. Yang, Non-Hermitian Skin Modes Induced by On-Site Dissipations and Chiral Tunneling Effect, *Phys. Rev. Lett.* **125**, 186802 (2020).
- [109] K. Yokomizo and S. Murakami, Topological semimetal phase with exceptional points in one-dimensional non-hermitian systems, *Phys. Rev. Res.* **2**, 043045 (2020).
- [110] Z. Yang, K. Zhang, C. Fang, and J. Hu, Non-Hermitian Bulk-Boundary Correspondence and Auxiliary Generalized Brillouin Zone Theory, *Phys. Rev. Lett.* **125**, 226402 (2020).
- [111] K. Yokomizo and S. Murakami, Non-bloch band theory in bosonic bogoliubov-de gennes systems, *Phys. Rev. B* **103**, 165123 (2021).
- [112] T.-S. Deng and W. Yi, Non-bloch topological invariants in a non-hermitian domain wall system, *Phys. Rev. B* **100**, 035102 (2019).
- [113] L. Li, C. H. Lee, S. Mu, and J. Gong, Critical non-hermitian skin effect, *Nat. Commun.* **11**, 5491 (2020).
- [114] S. Rafi-Ul-Islam, Z. B. Siu, H. Sahin, C. H. Lee, and M. B. A. Jalil, Critical hybridization of skin modes in coupled non-hermitian chains, *Phys. Rev. Res.* **4**, 013243 (2022).
- [115] C.-H. Liu, K. Zhang, Z. Yang, and S. Chen, Helical damping and dynamical critical skin effect in open quantum systems, *Phys. Rev. Res.* **2**, 043167 (2020).
- [116] S. Rafi-Ul-Islam, Z. B. Siu, H. Sahin, C. H. Lee, and M. B. A. Jalil, System size dependent topological zero modes in coupled topoelectrical chains, *Phys. Rev. B* **106**, 075158 (2022).
- [117] P. Calabrese and J. Cardy, Entanglement entropy and conformal field theory, *J. Phys. A: Math. Theor.* **42**, 504005 (2009).
- [118] T. Nishioka, S. Ryu, and T. Takayanagi, Holographic entanglement entropy: An overview, *J. Phys. A: Math. Theor.* **42**, 504008 (2009).

- [119] B. Swingle, Entanglement renormalization and holography, *Phys. Rev. D* **86**, 065007 (2012).
- [120] C. H. Lee and P. Ye, Free-fermion entanglement spectrum through wannier interpolation, *Phys. Rev. B* **91**, 085119 (2015).
- [121] Y. Gu, C. H. Lee, X. Wen, G. Y. Cho, S. Ryu, and X.-L. Qi, Holographic duality between $(2+1)$ -dimensional quantum anomalous hall state and $(3+1)$ -dimensional topological insulators, *Phys. Rev. B* **94**, 125107 (2016).
- [122] L. Herviou, N. Regnault, and J. H. Bardarson, Entanglement spectrum and symmetries in non-hermitian fermionic non-interacting models, *SciPost Phys.* **7**, 069 (2019).
- [123] C. Ortega-Taberner, L. Rødland, and M. Hermanns, Polarization and entanglement spectrum in non-hermitian systems, *Phys. Rev. B* **105**, 075103 (2022).
- [124] N. Okuma and M. Sato, Quantum anomaly, non-hermitian skin effects, and entanglement entropy in open systems, *Phys. Rev. B* **103**, 085428 (2021).
- [125] L.-M. Chen, Y. Zhou, S. A. Chen, and P. Ye, Quantum entanglement of non-hermitian quasicrystals, *Phys. Rev. B* **105**, L121115 (2022).
- [126] K. Kawabata, T. Numasawa, and S. Ryu, Entanglement phase transition induced by the non-hermitian skin effect, *Phys. Rev. X* **13**, 021007 (2023).
- [127] K. Yokomizo and S. Murakami, Scaling rule for the critical non-hermitian skin effect, *Phys. Rev. B* **104**, 165117 (2021).
- [128] L. C. Xie, L. Jin, and Z. Song, Antihelical edge states in two-dimensional photonic topological metals, *Sci. Bull.* **68**, 255 (2023).
- [129] M. Parto, Y. G. N. Liu, B. Bahari, M. Khajavikhan, and D. N. Christodoulides, Non-hermitian and topological photonics: optics at an exceptional point, *Nanophotonics* **10**, 403 (2020).
- [130] R. El-Ganainy, M. Khajavikhan, D. N. Christodoulides, and S. K. Ozdemir, The dawn of non-hermitian optics, *Commun. Phys.* **2**, 37 (2019).
- [131] B. Midya, H. Zhao, and L. Feng, Non-hermitian photonics promises exceptional topology of light, *Nat. Commun.* **9**, 2674 (2018).
- [132] H. Wang, B. Xie, S. K. Gupta, X. Zhu, L. Liu, X. Liu, M. Lu, and Y. Chen, Exceptional concentric rings in a non-hermitian bilayer photonic system, *Phys. Rev. B* **100**, 165134 (2019).
- [133] H. Wang, X. Zhang, J. Hua, D. Lei, M. Lu, and Y. Chen, Topological physics of non-hermitian optics and photonics: A review, *J. Opt.* **23**, 123001 (2021).
- [134] M. De Carlo, F. De Leonardis, R. A. Soref, L. Colatorti, and V. M. N. Passaro, Non-hermitian sensing in photonics and electronics: A review, *Sensors* **22**, 3977 (2022).
- [135] M. Hafezi, S. Mittal, J. Fan, A. Migdall, and J. M. Taylor, Imaging topological edge states in silicon photonics, *Nat. Photonics* **7**, 1001 (2013).
- [136] S. Mittal, V. V. Orre, G. Zhu, M. A. Gorlach, A. Poddubny, and M. Hafezi, Photonic quadrupole topological phases, *Nat. Photonics* **13**, 692 (2019).
- [137] K. Zhang, Z. Yang, and C. Fang, Correspondence between Winding Numbers and Skin Modes in Non-Hermitian Systems, *Phys. Rev. Lett.* **125**, 126402 (2020).
- [138] C. H. Lee and S. Longhi, Ultrafast and anharmonic rabi oscillations between non-bloch bands, *Commun. Phys.* **3**, 147 (2020).
- [139] B. Zhang, Q. Li, X. Zhang, C. H. Lee, Real non-Hermitian energy spectra without any symmetry, *Chinese Physics B*, **31**, 070308 (2022).
- [140] C. H. Lee and X.-L. Qi, Lattice construction of pseudopotential hamiltonians for fractional chern insulators, *Phys. Rev. B* **90**, 085103 (2014).
- [141] W. P. Su, J. R. Schrieffer, and A. J. Heeger, Solitons in Polyacetylene, *Phys. Rev. Lett.* **42**, 1698 (1979).
- [142] M. Atala, M. Aidelsburger, J. T. Barreiro, D. Abanin, T. Kitagawa, E. Demler, and I. Bloch, Direct measurement of the zak phase in topological bloch bands, *Nat. Phys.* **9**, 795 (2013).
- [143] L. Wang, M. Troyer, and X. Dai, Topological Charge Pumping in a One-Dimensional Optical Lattice, *Phys. Rev. Lett.* **111**, 026802 (2013).
- [144] M. Lohse, C. Schweizer, O. Zilberberg, M. Aidelsburger, and I. Bloch, A thouless quantum pump with ultracold bosonic atoms in an optical superlattice, *Nat. Phys.* **12**, 350 (2016).
- [145] S. Nakajima, T. Tomita, S. Taie, T. Ichinose, H. Ozawa, L. Wang, M. Troyer, and Y. Takahashi, Topological thouless pumping of ultracold fermions, *Nat. Phys.* **12**, 296 (2016).
- [146] M. Leder, C. Grossert, L. Sitta, M. Genske, A. Rosch, and M. Weitz, Real-space imaging of a topologically protected edge state with ultracold atoms in an amplitude-chirped optical lattice, *Nat. Commun.* **7**, 13112 (2016).
- [147] L. Li, C. H. Lee, and J. Gong, Impurity induced scale-free localization, *Commun. Phys.* **4**, 42 (2021).
- [148] M. Ezawa, Dynamical nonlinear higher-order non-hermitian skin effects and topological trap-skin phase, *Phys. Rev. B* **105**, 125421 (2022).
- [149] H. Jiang and C. H. Lee, Filling up complex spectral regions through non-hermitian disordered chains, *Chin. Phys. B* **31**, 050307 (2022).
- [150] C.-X. Guo, C.-H. Liu, X.-M. Zhao, Y. Liu, and S. Chen, Exact Solution of Non-Hermitian Systems with Generalized Boundary Conditions: Size-Dependent Boundary Effect and Fragility of the Skin Effect, *Phys. Rev. Lett.* **127**, 116801 (2021).